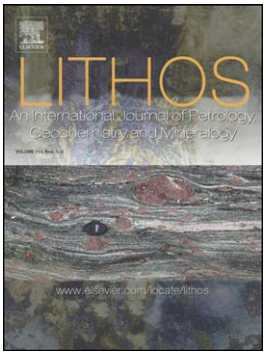

Geochemistry and radiogenic isotope characteristics of xenoliths in Archean diamondiferous lamprophyres: Implications for the Superior Province cratonic keel

D.A. Wyman, P. Hollings, R.V. Conceição

PII: S0024-4937(15)00067-5
DOI: doi: 10.1016/j.lithos.2015.02.018
Reference: LITHOS 3535

To appear in: *LITHOS*

Received date: 13 August 2014
Accepted date: 10 February 2015

Please cite this article as: Wyman, D.A., Hollings, P., Conceição, R.V., Geochemistry and radiogenic isotope characteristics of xenoliths in Archean diamondiferous lamprophyres: Implications for the Superior Province cratonic keel, *LITHOS* (2015), doi: 10.1016/j.lithos.2015.02.018

Geochemistry and radiogenic isotope characteristics of xenoliths in Archean diamondiferous lamprophyres: Implications for the Superior Province cratonic keel

Wyman, D.A. [1], Hollings, P.[2], and Conceição, R.V.[3],

[1]School of Geosciences, University of Sydney, Australia

[2] Geology Department, Lakehead University, 955 Oliver Rd, Thunder Bay, Ontario, P7B 5E1, Canada

[3]Laboratório de Geologia Isotópica, Universidade Federal do Rio Grande do Sul, Porto Alegre, Brazil

Corresponding author –Derek.wyman@sydney.edu.au

Abstract

Xenoliths retrieved from lamprophyric hosts in the Michipicoten belt fall into four groups defined by Al-Mg contents but do not include mantle peridotite. Based on immobile trace element abundances, the xenoliths are derived from magmas associated with the main phase of arc volcanism between 2.75 and 2.70 Ga or are co-genetic with the orogenic shoshonite suite.

Trace elements distinguish two styles of metasomatism characterized either by LILE enrichment or both LILE and Zr-Hf (± Nb-Ta). The first is likely associated with a hydrous fluid while the second is related to melts that permeated underplated shoshonitic mafic magmas and cumulates or the older sub-arc mantle. The Sm-Nd isotopic compositions of the xenoliths indicate that an aged, highly depleted, source was tapped during the orogenic event.

The formation depths of the lamprophyric magmas, and the xenoliths they contain, contrast with the calculated depths to the base of the depleted lithosphere based on xenoliths retrieved from post-Archean kimberlites. The differences imply a late docking of the ~ 150-160 km deep Archean keel beneath the Abitibi-Wawa terrane following the emplacement of major orogenic gold deposits.

Keywords; diamond, Archean, lamprophyre, shoshonite, xenolith, Superior Province

1. Introduction

Diamonds were discovered in Superior Province Archean shoshonitic lamprophyres in 1996 (Sage, 2000) and have been the focus of a number of publications since that time (e.g., Stott et al., 2002; Lefebvre et al., 2005; Stachel et al., 2006; Wyman et al., 2006; Kopylova et al., 2011). The diamond occurrences are now recognized across the southern margin of the Superior Province after mineral exploration identified occurrences in the central and eastern Wawa subprovince and the westernmost Abitibi subprovince (Stott et al., 2002) and a concerted effort by the Ontario Geological Survey to assess diamond occurrences in Archean lamprophyres of the Abitibi belt identified diamond-bearing examples from the Wawa subprovince boundary to the Quebec border (Gabrowski and Wilson, 2005). Diamonds were recovered from 6 of 45 lamprophyre sampled in the reconnaissance program. The number of diamonds recovered from the ~ 25 kg Abitibi lamprophyre samples ranged between 1 and 23. Given the limitations of sample size, however, the results indicate that non-economic diamond occurrences in thin (typically < 1 m wide) Archean lamprophyres are widespread across the southern Superior Province. Wyman et al. (2006) undertook a study of the diamond-hosting lamprophyres and the mafic – ultramafic xenoliths they contain. Many of those xenoliths were collected in a geographically restricted area in Lalibert Township (Fig. 1) and exhibited similar websterite major element and immobile trace element abundances, which provided an opportunity to assess metasomatic processes that resulted in coupled variations in incompatible element abundances and isotopic compositions. These websterites are

plotted in figures of the present paper as Group 1A, as described in a following section. The present study broadens the scope of the Wyman et al. (2006) xenolith chemical and isotopic database to better reflect the range of mafic – ultramafic xenolith types found in the diamond-bearing lamprophyres.

The results are used to characterize mantle and crustal processes associated with late Archean orogeny in the world's largest craton. The interpretations given here represent an extension of results and interpretations provided in previous papers (Wyman et al., 2006; O'Neill and Wyman, 2006; Wyman et al., 2008) where both a form of plate tectonics and mantle plume processes were inferred to co-exist. Nonetheless, a wide range of alternative models exist for Archean geodynamics, including some that argue strongly against mantle plumes (Anderson, 2013) and others that find "none of the indicators of Phanerozoic-type convergent and divergent plate interactions" in the Archean record (Hamilton, 2011, p. 4). Space does not allow a detailed assessment of these contrasting models but one aspect of the debate is particularly relevant to the present study. Opponents of Archean plate tectonics commonly cite the absence of blueschist and ultra-high pressure assemblages until the Neoproterozoic as evidence for their view (op. cit.). These features are products of the "cold finger" effect created by inserting relatively cool crust into the mantle. Our previous papers argue that the presence of diamonds in shoshonitic lamprophyres derived from the shallow mantle provides evidence of a similar effect in the late Archean (e.g., Wyman et al., 2008). Recently, Bédard and Harris (2014) have proposed a mantle wind-driven geodynamic scenario for the Superior Province and Minnesota River Valley terrane but that model does not appear to be consistent at 2.72

Ga with the presence of a komatiites along the Province's southern margin. The associated plume constitutes the most plausible source of mantle wind, but it would have acted to separate the Superior Province from Minnesota River Valley terrane. The present paper provides unique insights into these geodynamic controversies by identifying upper mantle rock types and metasomatic processes at the time of orogeny and consolidation of the Superior Province craton.

2. Regional Setting and Host Rock Models

2.1 Geological Setting

The Abitibi and Wawa greenstone belts define a continuous east-west granite-greenstone trend interrupted by the Kapuskasing tectonic zone, which exposes mid-crustal lithologies as a result of Early Proterozoic thrusting (Williams et al., 1991). As a result, they are now referred to collectively as the Wawa-Abitibi terrane (e.g., Stott, 2011). A U-Pb geochronological and Nd-Hf isotopic granite study by Ketchum et al. (2008) provides an indication that the Abitibi and Wawa belts developed in proximity to each other as had been widely inferred (e.g., Card and Ciesielski, 1986). They identified ca. 2850 Ma inherited zircons in both 2747 Ma tonalite and 2700 Ma granodiorite of the western Abitibi belt. The zircons displayed large intra-sample variations in $^{176}Hf/^{177}Hf$ that are consistent with the mixing of magmas derived from the mantle with or without juvenile crust and older crustal sources. In contrast, 2744 Ma and 2715 Ma tonalites from the south central part of the Abitibi belt 150 km east of the Kapuskasing structural zone lack zircon inheritance and display less intra-sample Hf isotopic variability in zircons (Ketchum et al., 2008). On this basis, old crust of the Wawa belt may have extended

eastward 75 km beneath the western Abitibi or alternatively sediments from the Wawa belt were deposited on to the developing Abitibi terrane. In either case, however, the eastern Wawa belt comprises assemblages ranging in age between 2.97 Ga and 2.7 Ga whereas pre-2.75 Ga crust has not been identified in the southern Abitibi (Ayer et al., 2002).

The Michipicoten and the western Abitibi greenstone belts both contain sequences of volcanic rocks consisting of combinations of komatiitic, tholeiitic and calc alkaline rock types. Williams et al. (1991) defined the Hawk, Wawa and Catfish assemblages in the MGB and they correspond to volcanic cycles 1, 2 and 3 described by Sage (1994) and Sage et al. (1996a), which have approximate ages of 2900 Ma, 2750 Ma, and 2700 Ma. The oldest cycle is dominated by a komatiite – basalt association, with some overlying felsic lithologies preserved, and occurs to the south of the younger rocks in the study area. Other komatiite-bearing sequences occur in the eastern Wawa belt in the Schreiber–Hemlo and White River–Dayohessarah greenstone belts to the west of the study area, but they have been interpreted as the accreted products of a younger plume that ascended in the vicinity of the southern Abitibi belt and peaked in terms of magma eruption rates at ~ 2.72 Ga (Polat et al., 1998; 1999, Wyman et al., 2002). Goldstein and Francis (2008) propose that many of the so-called Al-depleted komatiites of the southern Superior Province are actually ferro-picrites derived by the melting of an olivine dominated and trace element enriched mantle source.

The limited extent of the 2.9 Ga volcanism in the Michipicoten area suggests that the Hawk Terrane is a reworked "proto-craton". Small domains of older ≳ 2.9 Ga rocks are increasingly recognized in Neoarchean-dominated cratons or subprovinces worldwide. In the Superior Province, a small region of such rocks is recognized along the north-eastern margin of the Abitibi belt (Thurston et al., 2012) and Percival et al. (2012) proposed that the Hawk and several other terranes were initially distinct features that, by 2720 Ma, were embedded within the developing Superior craton or the fringing Wawa – Abitibi arc. The small Pontiac Terrane, which accreted to the southern margin of the Abitibi during a subduction-driven collision (Calvert et al., 1995), also has a ~ 3 Ga substrate, based on granitoid Pb isotopic studies and xenocrystic zircons found in sedimentary rocks (Carignan et al., 1983; Gariépy et al., 1984). Similar "microcontinents" are now also recognized in the Yilgarn Craton (Mole et al., 2014).

Sylvester et al. (1987) argued that the combination of incompatible element-depleted and enriched basalts in the 2.75 – 2.70 Ga cycles, the latter displaying variable relative Nb-Ta depletions versus Th and La, was consistent with a subduction zone setting. They suggested that the southern Superior Province at this time was broadly analogous to Phanerozoic arcs such as the Taupo-Kermadec-Tonga volcanic system in having subduction along both a continental margin and an oceanic arc segment. Late sedimentary rocks of the Doré metasediments (~ 2698 Ma – 2680 Ma) postdate cycle 3 and are considered to represent the erosional removal of felsic volcanic cap rocks from that cycle (Corfu and Sage, 1992; Rice and Donaldson, 1992).

A late contribution from an enriched mantle is noted in the youngest volcanic sequences of the north-eastern Wawa, possibly dated by xenocrystic ~2.716 – 2.700 Ga zircons in a ~ 2.691 Ga porphyry dike (Lodge et al., 2014), and may represent the appearance of a plume mantle component in the final stages of pre-orogenic mafic volcanism (Kerrich et al., 2008; Polat, 2009; Lodge et al., 2014). The results are consistent with the inferred relationship between the late Archean plume and the southern Superior subduction zone in the two areas. Plume ascent occurred directly beneath the Abitibi and plume mantle also leaked into the mantle wedge region of the southern Abitibi belt once subduction resumed (Dostal and Mueller, 1997, 2013; Wyman and Kerrich, 2009). In contrast, the plume did not rise directly beneath the 2.75 – 2.70 Ga eastern Wawa and post-2.72 Ga komatiite-bearing assemblages of the Wawa belt represent accreted material derived from outboard of the trench (Polat et al., 1998; 1999). Plume asthenosphere likely did spread along the arc, resulting in enriched components that were tapped late in the volcanic evolution of the Wawa belt (Lodge et al., 2014). The absence of younger plume volcanic sequences in the Michipicoten greenstone belt can be accounted for by the existence of the older Cycle 1 Hawk terrane outboard (to the south) of the 2.75 – 2.70 Ga arc sequences. If any of the younger plume sequences were accreted in this area, then they would lie even further south and have not been preserved.

Shoshonitic (monzonite, syenite, trachyte, lamprophyre) and sanukitoid (Mg-diorite, monzodiorites, trachyandesites: Shirey and Hanson, 1984) igneous rocks occur in both the Abitibi and Wawa subprovinces (e.g., the quartz syenite-quartz monzonite-granite and alkali feldspar syenite-alkali feldspar quartz syenite series of Feng and Kerrich, 1991; see

also Sage et al., 1996b). The shoshonite suite generally displays a late- to post-kinematic timing (Wyman and Kerrich, 1989; 1993) but Stott et al. (2002) noted that in the Michipicoten belt study area, syenitic intrusions, such as the 2673 ± 8 Ma Dickenson Lake stock, are syntectonic and are affected by the regional folding and flattening foliation. The shoshonitic lamprophyres of this suite have similar ages across the southern Superior Province. For example, Wyman and Kerrich (1993) reported a 2674 ± 2 Ma U-Pb titanite age for a lamprophyre near Kirkland Lake in the Abitibi belt and Stott et al. (2002) gave a 2674 ± 8 Ma titanite age for a lamprophyre from a Wawa diamond prospect.

Faure et al. (2011) have generated a three dimensional summary of the seismic architecture of the North American Archean mantle between 30 and 250 km depths and showed that the shallowest portions of these keel structures are typically a few 100 km wide. Their results illustrate that the northeastern and northwestern parts of the Superior Province craton are underlain by the thickest cratonic root (225 – 240 km) whereas the southern, mainly younger, terranes are underlain by a thinner subcontinental lithospheric mantle (SCLM) with the depth of the depleted lithosphere estimated at 160 km for Kirkland Lake in the Abitibi belt and 150 km in the eastern Wawa region (Kaminsky et al., 2002; Griffin et al., 2004). A study of post-Archean kimberlite-borne garnet xenocrysts by Scully et al. (2004) revealed abrupt changes in calculated mantle chemistry across major fault structures of the southern Superior Province as measured by xenocrystic garnets sampled by kimberlites that were only kilometres apart. In general, however, the southernmost part of the Superior Craton is underlain by comparatively

fertile mantle, which in the Faure et al. (2012) model has velocity perturbations between 4 and 6% compared to 6 to 8% in the cratonic core. The Michipicoten area lies to the south of the axis of the Delta Vd low and displays a velocity perturbation of ~ 5%. The region of relatively thin and fertile mantle corresponds closely to the distribution of large and giant orogenic gold deposits and lamprophyre-hosted diamonds in the southern Superior Province. Wyman et al. (2008) argued that the presence of diamonds and gold deposits was not coincidental, based on a recurring association in the Kaapvaal Craton and Slave Province and in post-Archean settings where deep cratonic roots were not present beneath orogenic gold provinces (Paleoproterozoic West Africa and Guyana, Proterozoic Australia, and the western US Mother Lode trend).

2.2 Timing of Diamond-Related Magmatism

Unfortunately, there are two very different interpretations concerning some of the most important Archean diamond host rocks in the southern Superior Province. The largest numbers of diamonds retrieved from Archean aged rocks in the Wawa and Abitibi belts are found in a conglomerate and in mafic – ultramafic bodies that have dimensions of 10s of meters by 100's of metres (maximum length ~ 4 km: Lefebvre et al., 2005). As summarised by Stott et al. (2002), "clasts within heterolithic breccias, which are locally closely (genetically?) associated with these dikes, are concentrated in bands and resemble volcaniclastic debris flow units. However, in the Enigma property ….. the heterolithic breccia units appear to transect the surrounding volcanic rocks, including dacitic lapilli tuff and pillowed basalt." (Stott et al., 2002, p. 9-1). Several studies by the Ontario Geological Survey (e.g., Vaillancourt et al., 2005a and references therein) have provided

evidence of the intrusive nature of these diamond host rocks, including: i) a planar preferred alignment of minerals at breccia contacts that was developed during emplacement as dikes ii) a train of clasts that resemble a dismembered dike, similar in composition to the adjacent foliated syenite pluton, iii) local intrusion of heterolithic breccia into syenite breccia that is itself intruded by syenite dikes containing ultramafic fragments, iv) a dismembered syenite dike within heterolithic breccia unit, v) intrusion of heterolithic breccia into syenite, vi) an apophyse of heterolithic breccia within syenites, vi) lamprophyre dikes (<2679.2±2.1 Ma, probably ~ 2674 Ma, based on U-Pb dates for other Wawa and Abitibi lamprophyres) that cross cut and occur within the breccias, locally display contacts that appear to merge and coalesce with the heterolithic breccias, and vii) a compositional continuum between the breccias and the dark lamprophyric rocks with intermediate units containing variable amounts of fragments and a lamprophyric matrix.

In contrast, Lefebvre et al. (2005) considered the heterolithic breccias to be volcaniclastic in nature. They describe the same rocks as massive, unstratified and poorly sorted in terms of clast size and density but with bedding planes that can be identified by variations in clast abundance or the relative abundance of felsic metavolcanic fragments. They reported that the tabular to wedge shaped beds are up to 10 m long and 0.3–1m thick and are massive or display only subtle grading. Kopylova et al. (2011) provide four U-Pb zircon geochronological results for an inferred “volcaniclastic” breccia. Four discordant results have ages greater than ~ 2684 Ma but one concordant zircon recovered from the breccia matrix gave a concordant age of 2619.06 ± 1.76 Ma.

To the extent that it suggests magmatism over a protracted period, this younger age appears to support the volcaniclastic model for the origin of the diamondiferous breccias. There are a number of factors, however, that suggest this is not the case. First, a granitic sill in the Gamitagama Lake greenstone belt, 50 km south of Wawa, has been dated at 2615 ± 10 Ma (Krogh and Turek, 1982), indicating a possible contact metamorphic mechanism for late zircon growth in the region. Secondly, it is known that zircon growth in the mid-crust of the amalgamated Abitibi – Wawa terrane continued for a prolonged period following orogeny and that quartz vein formation and hydrothermal activity occurred on existing structures in the Michipicoten belt through to 2630 – 2580 Ma (Moser, 1994). A comparison of the 1:20,000 map of Vaillancourt et al. (2005b) and the young age date location on the map of Kopylova et al (2011) suggests that the nearest diamond localities are those which Wilson (2005) describes as restricted to one of the recumbent nappes in the area where "thrusting and shortening may be related to the tectonic events along the Kapuskasing Structural Zone".

Geological context also suggests that the volcaniclastic model is implausible because it requires that similar unusual units erupted over a small (17 km x 18 km) area between 2743 ± 43 Ma to 2619.1 ± 1.8 Ma, indicating a minimum age span of about 80 m.y. Unlike repeated dike intrusion into a stable craton, the scenario requires that similar mantle magma sources were available despite a transition from pre-orogenic to orogenic and post-orogenic settings. The magmas would also be required to ascend through crust that underwent at least five distinct tectonic episodes of thrusting, folding, shearing,

compression, extension, and granulitization during the 80 m.y. (Moser, 1994).

There is greater consensus that one MGB diamond occurrence, the Leadbetter property, is a sedimentary occurrence corresponding to a fluvial conglomerate of the Doré metasedimentary rocks (Wendland et al., 2012). Kopylova et al. (2012) reported four U-Pb zircon ages from a dike that cross cuts the conglomerate. Three zircons returned similar $^{207}Pb/^{206}Pb$ ages of ~ 2691 to 2696 Ma and fourth zircon gave an age of 2685.4 ± 1.59 Ma. Kopylova et al. (2012) interpreted the age of the dike to be 2697.2 ± 1.8 Ma based on a three point regression of the first three ages but considered the fourth zircon to have undergone a distinct Pb loss episode because it did not fall on the same linear trend. Given the common occurrence of 2698 Ma detrital zircons in the Doré metasedimentary rocks (Corfu and Sage, 1992), an alternative interpretation is that the dike magma inherited zircons from the conglomerate and that, at this locality, it is ~ 2685 Ma or younger. The Leadbetter conglomerate occurs within 10 – 15 km of numerous diamond-bearing lamprophyric breccias (Fig. 1). Referring to Helmstaedt et al. (2010), Kopylova et al. (2012) note that "the latter were presumed to be sourced from the lamprophyric breccias simply because of their spatial and temporal coincidence, even though the breccia's bulk compositions differ from that of the metaconglomerate" (p. 215). They prefer a kimblerlitic source, possibly 100's or up to 1000 km to the north and now completely eroded. They attribute the very restricted distribution of diamonds within the Leadbetter conglomerate to rapid erosion of the kimberlite and diamond deposition over a short time interval. Stachel et al. (2006) rejected this type of scenario on the basis that the diamonds show no surface features consistent with transport over long distances. The

main mineralogical evidence in support of the kimberlite host theory is the presence of diamond, picroilmenite, pyrope and ± corundum in heavy mineral separates. The first of these indicator minerals have been found in lamprophyric rocks as noted above. In addition, Kopylova et al. (2012) note "More information on picroilmenite compositions from ultramafic lamprophyres…… needs to be collected to unequivocally determine the host rock for metaconglomerate ilmenite" (p. 219). Unfortunately, there has not been an industrial-scale heavy mineral study of the MGB lamprophyric dikes and breccias comparable to that undertaken on the Leadbetter property and therefore the significance of the metaconglomerate heavy mineral assemblage is unconstrained by studies in the area. It is important to recognize, however, that diamonds were unknown in shoshonitic lamprophyres until comparatively recently and "anomalous" occurrences of other kimberlite indicator minerals such as high-Cr ilmenite are known from much younger lamprophyres (the Thumb minette: Griffin et al., 1998; Kopylova et al., 2012).

More importantly, a relevant heavy mineral analyses has been undertaken at the Dachine (French Guina) diamond locality. The weathered and schistose Dachine diamond host rocks were initially interpreted as alkalic dikes (S-S Sun pers comm., 2000; references in Bailey, 1999) but were later interpreted as pycroclastic komatiites (e.g., Capdevilla et al. 1999). Wyman et al. (2008) demonstrated, however, that the host rocks were compositionally equivalent to the matrix of the Wawa lamprohyric breccias. Picroilmenites with TiO_2 contents of 49 – 50 wt.% and MgO contents of 6.1 - 10.6 wt.% from Dachine (Bailey, 1999) overlap the kimberlite field cited by Kopylova et al. (2012) and the trend defined by their Leadbetter examples (Fig. 2). Bailey (1999) describes four

groups of pyrope garnets recovered from the Dachine diamond host. One of these groups displays complete overlap with those described by Kopylova et al. (2012). Accordingly, the suite of "kimberlitic" heavy minerals identified by Kopylova et al. (2012) is most reasonably attributed to the nearby diamondiferous lamprophyre occurrences as concluded by Stachel et al. (2006), Helmstedt et al. (2010) and Wendland et al. (2012).

On the basis of the evidence summarized here, the working hypothesis for the present paper is based on the following points:

1. Southern Superior Province diamondiferous lamprophyres are related to a late tectonic shoshonite – sanukitoid suite emplaced at around 2674 Ma
2. Diamond-bearing heterolithic breccias are genetically and temporally related to the lamprophyre suite, which accounts for the compositional overlap and mutually cross-cutting field relationships. In the MGB, both rock types were emplaced during late orogenic deformation.
3. The vast majority of breccias recognized in the field are intrusive in nature, although the possibility of a volcaniclastic occurrence at a ~ 2674 Ma paleo-surface is not excluded.
4. There is no unequivocal evidence in support of Archean kimberlites in the Superior Province Craton and the mantle xenoliths and heavy mineral suite associated with the diamonds in the MGB were entrained by nearby shoshonitic magmas over a narrow time interval corresponding to orogeny in the southern part of the Craton.

3 Petrographic Characteristics

The xenoliths have all undergone alteration and greenschist facies or higher-grade metamorphism, which commonly obscures primary mineralogical features, although phenocryst zoning, kinking of micas and some other features are locally preserved (see Supplementary Figure 1; Wyman et al., 2006). Mafic xenoliths are characterized by varying combinations of mainly secondary amphibole and mica and/or chlorite that pseudomorph primary phases or occur as aggregates that overprint primary textures. The groundmass is feldspathic but may contain fine-grained carbonates and accessory titanite, oxides and sulphides. Ultramafic samples generally have a talc-rich groundmass and relict micas, commonly chloritized. Several samples (e.g., WX 8 and 9) contain isolated euhedral carbonate grains that partially preserve early micas.

4 Geochemical Results

Methods are described in Appendix 1. Whole-rock major and trace element data for MGB Archean lamprophyre-hosted xenoliths are given in Table 1. The results display a wider range of xenolith compositions than reported in Wyman et al. (2006) and are grouped according to Mg# and Al_2O_3 contents, consistent with published classification schemes for lower crust and upper mantle xenoliths (e.g., Berly et al., 2006). Isotopic results for a subset of the samples are given in Table 2.

4.1 Major Element-Based Sub-Groups

Based on the plots of Al_2O_3 vs Mg# or MgO (Fig. 3b), which include data from Wyman et al. (2006), three main groups of xenoliths are present along with one unique sample.

For ease of discussion, these are referred to as Groups I through IV. None of the Groups display the high MgO content (> 35 wt.%) that is characteristic of peridotites (Pearson et al., 2003). The previously reported websteritic samples are part of a low-Al Group I trend that is similar to crustally-derived pyroxenites, commonly of cumulate origin (Berly et al., 2006). The new Group I samples and previously reported websterites of Wyman et al. (2006) have broadly similar major and immobile trace element compositions but do not overlap in all respects. For example, the new samples have Al_2O_3 contents of 3.3 to 4.9 wt.% whereas the previous samples are restricted to 1.2 to 2.5 wt.% (Fig. 3). For ease of reference, and to avoid confusion related to the existing "high Al – low Al" terminology for websterites, the previously described samples are referred to as Group IA and the new samples as Group IB.

Despite partially overlapping MgO contents and Al_2O_3/TiO_2 values, Groups I and II can be distinguished on a number of MgO variation diagrams employing Ni, Al_2O_3, etc. (Fig. 3). Groups II and III extend to higher Al_2O_3 contents than the Group I xenoliths (Fig. 3a,b). Group II have mainly basaltic MgO contents of 11.5 to 22.0 wt.% and Al_2O_3 contents between ~ 6 and 12 wt.%. These and other major element oxide abundances partially overlap with those of shoshonitic lamprophyres and the nearby ultramafic Deep Lake stock (Wyman et al., 2006). Group III have Al_2O_3 contents between 1 and 8 wt.% and higher but relatively restricted MgO contents between 27.6 to 30.0 wt.% that are too low for mantle peridotites (Bodiner and Godard, 2003). These compositions are generally associated with mantle pyroxenites formed by reaction of the upper mantle with

ascending magmas (Garrido and Bodinier, 1988; Berly et al., 2006). The single Group IV sample also falls in the mantle pyroxenite field (Fig. 3).

4.2 Trace Element Characteristics

Trace element contents reveal a greater diversity within the xenolith population. In terms of compatible elements, the entire xenolith data set defines two trends on a Co vs Ni plot and the Group I xenoliths fall on both of these (Fig. 4a). A plot of Sc/V vs Ti/V also indicates that some Group II xenoliths with low Ti/V fall off of a trend defined by shoshonitic lamprophyre host rocks and other xenoliths from the Group (Fig. 4). Previously studied Group 1A websteritic xenoliths showed similar contents of the high field strength elements combined with highly variable LREE-MREE abundances and overall REE fractionation (Wyman et al., 2006). Group 1B, however, shows a far greater variation in Zr content, for example, compared to 1A xenoliths.

Primitive mantle normalized multi-element plots (Fig. 5) are used to summarize the trace element characteristics of the xenolith groups. Compared to the previously published data for Group 1 samples, the new samples are more diverse, even when a single locality is considered. Sample WX-19 is distinct in having the highest incompatible element contents and a relatively monotonous increase in abundance of lighter REE (Fig. 5a). Five other Group 1 samples display slight to significant concave upward MREE-HREE patterns. Among the latter samples, relative Nb depletions versus neighbouring La and Th are present in three examples (Fig. 5a). Two other samples exhibit decreasing normalized REE abundance from the HREE to the MREE (WX-17, WX-21) and minor positive and

negative Nb anomalies. In contrast to other Group 1 samples, these two examples do not exhibit negative Zr-Hf anomalies (Fig. 5a).

The majority of Group II samples (Fig. 5b) display primitive mantle normalized patterns that are typical of their shoshonitic lamprophyre hosts in terms of HFSE anomalies, LREE enrichments and overall trace element contents (Wyman et al., 2006). Three other samples display less overall fractionation and more closely resemble arc tholeiite rock types, although one has a prominent positive Eu anomaly suggesting that it contains cumulate plagioclase (WX-18, Eu/Eu* = 1.5).

Group III samples (Fig. 5c) define a relatively homogeneous set of normalized patterns that resemble the dominant subgroup of Group II xenoliths. They are distinguished, however, by overall trace element contents that are mostly an order of magnitude lower. In contrast to Group II, which has high normalized Lu/Al and V/Al, the Group III samples display much lower values for these ratios (i.e., they have "positive" Al anomalies). In addition, Nb depletions are generally much more pronounced in the Group III xenoliths. Figure 6 illustrates that, with a few outliers, the three main xenolith groups define distinct trends on a Nb/Nb* versus Al_2O_3 plot and that only Group II significantly overlaps the trend defined by the shoshonite (lamprophyre and syenites) host suite. The normalized plot of the single Group IV xenolith resembles the most incompatible element-depleted samples of Group III but displays a positive Ti anomaly not observed in the other group.

4.3 Isotopic Compositions

Given that no direct age estimates are available for individual xenoliths or xenoliths groups, whole rock Sm-Nd isotopic results are expressed in terms of $\varepsilon Nd_{T= 2674Ma}$ based on the emplacement ages of shoshonitic lamprophyres in the eastern Wawa subprovince and Abitibi subprovince. The resulting εNd_T values extend over a wide range from -3.3 to 29.7 (Fig. 7a). Two outlier (?) results at high εNd_T (~ 25-30) preclude any Nd-εNd_T group trends in the new isotopic data. New Group IB results, however, clearly do not follow the trend of previously reported 1A websterites. Figure 7 includes representative analyses of a Wawa Subprovince lamprophyre and a Cycle 3 volcanic rocks (Wyman et al., 2006), which are typical of their respective lithologies in the southern Superior Province, falling within a more restricted range of εNd_T values than documented in the xenoliths.

A plot of $^{207}Pb/^{204}Pb$ versus $^{206}Pb/^{204}Pb$ defines an array that mainly overlaps previously reported data (Fig. 7b). Sample WX-2 lies above the trend. It is one of two Group III samples on the primitive mantle normalized plot (Fig. 5c) that crosscut trends of other samples where the LREE contents are "too high" versus the HREE, based on other xenoliths in the group. The other crosscutting sample (WX-3) was not analysed isotopically. Apart from WX-2, there is no evidence that samples may have been isotopically modified by late fluids linked to uplift along the Kapuskasing Structural Zone. The xenolith $^{206}Pb/^{204}Pb$ compositions bracket the range defined by lamprophyre samples. As noted by Wyman et al. (2006), this relationship rules out the lamprophyre magmas and volatiles as significant metasomatic agents on the xenoliths. Data for Wawa

belt ore deposits (mainly galena analyses: Thorpe et al., 1987) and Cycle 1 and 2 whole rock data (Thorpe, 2008) are shown for comparison.

5 Discussion

The study of xenoliths in the Archean lamprophyres has the benefit of a known orogenic geodynamic context for the samples within the evolution of the southern Superior Province. The main drawback associated with these particular samples is their long residency at or near the Earth's surface and the resulting associated alteration. Based on comparisons of immobile major and trace elements, however, it is possible to infer many important early (pre-entrainment or entrainment) features of the main xenolith Groups.

5.1 Comparisons with Massif Samples and Xenoliths in Post-Archean Host Rocks

The Al and Mg contents of new and previously described Group I samples preclude a cognate (lamprophyric magma) origin. Instead, they closely resemble the arc-related crustal pyroxenite xenoliths found in younger host rocks. The consistent HFSE characteristics of the previously reported Group IA samples, combined with a trend to higher εNd_T at greater LREE contents, indicates that they originally had arc tholeiite-like characteristics (LREE depletion, minor negative to positive Nb and negative Ti anomalies), prior to a late metasomatic event involving REE-bearing fluids from a depleted source (Wyman et al., 2006). The eight new Group IB samples include two (WX-17, -21) that display HFSE-REE abundances similar to the least overprinted (lowest εNd_T) of the Group 1A websterites with contents near primitive mantle values. Another sample (WX-19) exhibits slight LREE enrichment along with relative Nb and moderate

negative Zr-Hf and Ti anomalies that are also consistent with an arc tholeiite precursor. The sample is distinguished by the highest incompatible element contents (Fig. 5a) combined with the lowest compatible element abundances in the group (Ni = 600 ppm). All Sm-Nd isotopic data for new Group I samples fall within the normal range of southern Superior Province volcanic rock types (εNd_T = 1 to 3: e.g., Polat and Kerrich, 2002), indicating that they have not been overprinted by the depleted-source fluids identified in the Group 1A samples.

Based on mineralogical and compositional studies, plus field relations with associated pyroxenites, Berly et al. (2006) argue that Solomon Island websterites are actually of mantle origin despite having low-Al arc websterite compositions and were the product of fluid mediated metasomatism linked to the subducted slab. They cautioned that similar processes may have occurred elsewhere. The Wawa Group I xenoliths lack the bell-shaped normalized REE profiles of the Solomon examples but nonetheless provide evidence of a role for fluids, based on their REE – HFSE systematics. Collectively, the data implies that non-shoshonitic websterites existed beneath the Wawa terrain prior to late tectonic magmatism but were sporadically overprinted by high εNd_T fluids liberated during orogeny. The fluids may have been liberated from strongly depleted 2900 Ma Cycle I shallow mantle sub-arc sources during the later orogeny, as suggested by Wyman et al. (2006), but high εNd_T compositions could also be generated over a few 10's of m.y. from younger sub-arc sources.

Group II xenoliths also include three examples with primitive mantle-normalized plots

that resemble arc tholeiites or typical eclogites (e.g., Pearson et al., 2003), but the majority exhibit strong LREE enrichments and pronounced HFSE anomalies. Both of these types have been recovered from the WX area and even from the same host dike. Eclogite xenolith suites from a single locality commonly display a range of compositions. Barth et al. (2001, 2002) divided eclogite xenoliths from the Koidu kimberlite complex, Sierra Leone, into low – MgO and MgO groups, based on a compositional gap between 13 wt.% and 15 wt.% MgO. Although the Wawa Group II samples extend across a similar range of MgO contents, they do not display the gap noted in the Koidu kimberlite sample set. Compared to previously published compilations, however, the high-MgO Wawa Group II xenoliths are distinctive in having low Al_2O_3 (less the 10 wt.% versus mainly 10 -20 wt.%).

Pearson et al. (2003) note the compositions of many xenolithic eclogites do not correspond to those of typical Archean volcanic rock types and typically have low SiO_2 contents for their respective MgO. A popular model to account for the differences in eclogite xenolith compositions globally, compared to massif eclogites or common volcanic rock types, invokes Archean slab melting to produce the tonalite-trondhjemite-granodiorite (TTG) from the mafic rock precursors of xenolith eclogites (Jacob and Foley, 1999; Barth et al., 2001, Pearson et al., 2003). The Group II xenoliths, however, overlap both common Wawa Subprovince volcanic rock types and the shoshonitic lamprophyre compositions. This overlap raises the possibility that some Group II xenoliths are of shallow crustal origin or are mafic enclaves rather than true eclogites. Pyroxene zoning in evolved minettes in the Abitibi belt provides evidence of mixing

between batches of lamprophyric magmas (Wyman and Kerrich, 1993) while textural evidence for "pilite" olivine cumulates and geochemical data indicate that the most Mg-rich of the Wawa lamprophyres have inherited excess olivine (Wyman et al., 2006). Analyses of mafic enclaves in the multi-phase shoshonitic Otto stock of the Abitibi belt indicates that those inclusions compositionally overlap both Groups I and high-Mg Group II xenoliths (A. Temelkovski, Lakehead University, pers. comm. 2014). Given that i) the other Wawa xenoliths groups are mantle-derived, ii) basaltic volcanic rocks with shoshonitic signatures do not occur in the area (i.e., the xenoliths are not shallow crustal "country rock"), and iii) the presence of diamonds and the eclogitic mineral inclusions in these diamonds (De Stefano et al., 2006), it is probable that some of the xenoliths would have qualified as eclogitic on the basis of their mineral assemblage at the time of entrainment. In any case, the "shoshonitic" xenolith compositions do not suggest a link to prior slab melting, and appear unrelated to TTG magmatism, which predated the shoshonite suite (Sage et al., 1996b).

Alternative models of Archean eclogite xenolith formation are now commonly invoked (Jacob, 2004; Gonzaga et al., 2010 and references therein). For example, some authors argue for subcrustal underplating of mafic magmas and eclogite formation from the metamorphism of the resulting mafic lower crust (e.g., Griffin and O'Reilly, 2007). In this scenario, which appears more plausible for the present case, the Wawa mafic xenoliths are mainly "cognate" in nature, being derived from underplated magmas associated with the late shoshononitic syenites, monzonites, lamprophyres and trachytes found across the Superior Province but particularly abundant along the craton's southern

margin. In this interpretation, Group II xenoliths were likely derived from depths similar to those associated with "sub-arc" Group I websterites (Wyman et al., 2006). The Nd isotope systematics in Group II xenoliths are considered along with those of Group III.

Group III xenolith compositions are distinct from shoshonitic lamprophyres in having higher MgO and lower Al_2O_3 contents (Fig. 3a). The xenoliths fall in the mantle peridotite field and partly in the region of overlap with arc-related crustal pyroxenites (Fig. 3b; Berly et al., 2006). The uniform trace element signatures and well-defined trends on numerous variation diagrams, however, strongly suggest a common mantle origin for the Group. They display relatively consistent normalized multi-element patterns and incompatible element ratios (e.g., $[La/Sm]_N$) at highly variable overall incompatible element contents, although Nb anomalies and absolute concentrations do distinguish samples WX1 and WX2 (Nb = 1.60 and 1.02 ppm) from other samples (0.06 to 0.26 ppm). The range of Group III MgO contents is relatively restricted (28 to 30 wt.%) over a wide range of SiO_2 abundances (52 – 61 wt.%) and Ni (2616 ppm to 1475 ppm) and are compensated for mainly by strong negative correlations between SiO_2 and Fe_2O_3, Al_2O_3, and TiO_2. These compositions are also distinctly higher than those found in minor shoshonitic intrusions of the southern Superior Province (e.g., hornblendite and pyroxenite phases of the Abitibi Otto stock: < 17.7 wt.% MgO; Berger, 2006).

Although the major element contents of the Group III xenoliths broadly correspond to those of certain previously published arc-related pyroxenite occurrences in younger settings, they differ from most in their trace element characteristics. Most rock types in

the Ronda Massif display strong depletions of the more incompatible elements (Garrido and Bodinier, 1999) as do the great majority of Solomon Island supra-subduction zone pyroxenite xenoliths described by Berly et al. (2006). Similar combinations of LILE enrichment and relative HFSE depletions are reported, however, from the Bearpaw Mountains minette-hosted xenolith suite (Downes et al., 2004) that includes tectonite peridotites, cumulate mica peridotites and mica pyroxenites. Among these suites, the mica peridotite cumulate xenoliths, considered to be cogenetic with the host Bearpaw Mountain minette magma, exhibit some overlap with the Wawa Group III suite in terms of MgO and Al_2O_3 contents. Unlike Group III samples, however, they define a common igneous negative correlation between Al_2O_3 and MgO, along with the Group II metamorphosed mafic xenoliths, lamprophyre host rocks and Ronda recrystallized pyroxenites (Fig. 4a).

Accordingly, Mg-Al systematics and other chemical trends distinguish the majority of Wawa Group III xenoliths from other arc-related pyroxenite xenolith suites. Straight trends on many element-element plots suggest that the distribution of Group III xenolith compositions requires some form of mixing. Whereas Group II xenoliths and host lamprophyres define a "fractionation" trend on a plot of Th/Nd versus Th (Schiano et al., 2010; Fig 8), the low-Nb Group III xenoliths define a curve consistent with mixing between two end members similar to sample WX-10 (63 wt. % SiO_2, 1.4 wt.% Al_2O_3, 30 wt.% MgO, Th/Nd = 0.32) and WX-14 (52 wt.% SiO_2, 8.3 wt.% Al_2O_3, 28 wt% MgO, Th/Nd = 0.07).

We suggest that the low-Al end member likely represents arc cumulate pyroxenite originally formed during the ~ 2700 Ma Cycle 3 volcanism that predated syn-tectonic shoshonitic magmatism. It has very low K contents (0.01 wt.% K_2O) compared to other xenoliths in Group III or other xenoliths in the same host dike, but may have been modified by metasomatic fluids during orogeny, based on its high SiO_2 contents, LREE enrichment and normalized enrichment of Th versus Nb or La.

The high-Al end member resembles mantle pyroxenites in terms of Al and Mg# but its trace element profile closely matches the host shoshonitic lamprophyres. Downes et al. (2004) noted such similarities between cumulate mica peridotites, mica clinopyroxenites and the Eocene Bearpaw minettes and inferred a genetic link. Although the Wawa Group III xenoliths have SiO_2 contents more similar to Solomon Island pyroxenite xenoliths attributed to metasomatism of mantle peridotites by Berly et al. (2006), their Al_2O_3 contents are significantly greater (Solomon Islands 0.7 to 2.7 wt.% Al_2O_3 versus Low-Nb Group III 2.3 to 8.3 wt.% Al_2O_3) and most plausibly reflect a component that is co-genetic with the syn-orogenic shoshonitic magmas of the southern Superior Province. The two high-Nb samples display an even closer resemblance to the host magmas in terms of their overall incompatible element contents and major element characteristics and are also interpreted as being genetically related to the shoshonite magmas.

The single Group IV sample has very high LOI (~ 12 wt.%) and contains abundant carbonate, which may account for its relatively pronounced spoon-shaped or sinusoidal REE pattern compared to any other Wawa xenoliths, and the presence of minor positive

Zr-Hf and Ti anomalies on a primitive mantle-normalized plot. High LOI contents are relatively common in massif and mantle xenoliths samples (e.g., Downes et al., 2004; Van der Wal and Bodinier, 1996; Varfalvy et al. 1997; van der Meer et al., 2013) and the sample warrants inclusion in the study because of its distinctive composition, which includes elevated Al_2O_3 content (17.5 wt.%, recalculated volatile-free) similar to that of Ronda Massif garnet pyroxenites (Marchesi et al., 2013).

5.2 Significance of Xenolith Pb-Pb Isotopic Trends and High εNd_T Values

A comparison of the xenolith whole rock Pb-Pb compositions with those of Wawa greenstone belt whole rock data and hydrothermal ore deposit galena separates provides important insight into the origin of the xenoliths. The ~ 2.9 Ga Cycle 1 rocks define a distinct trend on a plot of $^{207}Pb/^{204}Pb$ vs $^{206}Pb/^{204}Pb$ (Fig. 7B) and 2.75 Ga Cycle 2 rocks mainly define a second trend that lies close to the single 2.70 Ga Cycle 3 volcanic sample and 2.68 Ga lamprophyres. The presence of some Cycle 2 rocks along the trend of 2.9 Ga rocks can plausibly be attributed to sporadic reworking of the older sequences during younger volcanism. Hydrothermal deposit galenas fall at low $^{206}Pb/^{204}Pb$ on both trends, but their compositions are influenced by the age of the local host rocks rather than their inferred absolute age (Thorpe et al., 1987). The restriction of all but one xenolith to the trend of 2.75 – 2.68 Ga volcanic and intrusive rocks suggests that they are derived from similar sources and have not been strongly altered by fluids or melts derived from lithosphere related to the 2.9 Ga Cycle 1 Hawk Terrane.

The Sm-Nd isotope systematics of the new Group II and III samples are notable for the high $\varepsilon Nd_{T=2674Ma}$ values, particularly for two samples (Group II WX4: +29.7; Group III WX1: +24.6). Wyman et al. (2006) reported that Group IA websterites with similar HFSE contents displayed increasing $\varepsilon Nd_{T=2674Ma}$ with higher LREE contents, although the trend appeared to "plateau" as $\varepsilon Nd_{T=2674Ma}$ values approached ~ 10. The new samples are more varied in terms of immobile HFSE but mainly define a trend to decreasing $\varepsilon Nd_{T=2674Ma}$ at greater Nd contents. When all of the Nd isotopic compositions are plotted against La/Sm, two possible trends are present. One is vertical at ~ $[La/Sm]_N$ = 2.5 and consists of Group II and III samples and the other defines a positive correlation between $[La/Sm]_N$ and includes samples from Groups I, II, and III (Fig 9a).

High εNd_T are well documented in mantle xenoliths and refractory sub-arc rocks. Pyroxenites and high-Al websterites of the Beni Bousera Massif had εNd_T ranging between −9 and +26, at their emplacement age of 21 Ma (Pearson et al., 1993) and εNd_T up to +500 are reported from eclogite xenoliths in kimberlites at the time of emplacement (Jacob, 2004). Other examples include i) isotopically heterogeneous mineral separates from Siberian Craton xenoliths where εNd_T extend from -55 to + 491 and ii) a 350 range of εNd_T variation in peridotite xenoliths from the Mir and Udachnaya kimberlites (Pearson et al., 1995). Aulbach et al. (2013) reported the isotopic compositions of mineral separates and calculated whole rocks for xenoliths retrieved by kimberlites from various depths in the stratified lithosphere of the Slave Craton. They showed that while xenoliths from the deep SCLM had undergone metasomatic modification and homogenization, rare xenoliths from the shallow SCLM retained strong isotopic heterogeneity. Garnets from

shallow mantle pyroxenites had εNd_T at the time of kimberlite eruption (55 Ma) ranging from -74 to + 54. Aulbach et al. (2013) conclude that samples from the shallow SCLM preserved signatures related to its ancient formation and to Proterozoic or earlier metasomatism by highly LREE-enriched low volume melt with marked Ti–Zr–Hf depletions, similar to carbonatite.

The global evidence from mantle xenoliths demonstrates that high εNd_T comparable to those of the Wawa xenoliths do occur in samples that have been relatively undisturbed since the emplacement of their mainly kimberlitic host rocks. In the case of the Wawa samples, however, the xenoliths were collected in outcrop, which raises the possibility that high εNd_T values in these samples have a mantle origin but that one or both of the trends versus La/Sm (Fig. 9a) represents disturbance since emplacement of the lamprophyre dikes. Although the two samples with the highest εNd_T values were collected from the same locality, two other samples from the same host rock do not display high values (Group II WX 4= 29.7, WX 5= 2.2; Group III WX 1: 24.6, WX 3 = 6.1).

If all of the xenolith samples are plotted against Ce/Ce*, commonly used to assess late REE mobility, then two trends are again defined but the vertical trend at "undisturbed" Ce/Ce* $\approx$ 1 includes the most unusual high εNd_T samples (Fig. 9b). The second trend displays a slight negative correlation between $\varepsilon Nd_{T=2674Ma}$ and Ce/Ce* but the ~ 0.7 to 1.1 range of the Ce anomaly can be attributed to variable LREE enrichment rather than distinct Ce troughs or peaks on normalized plots. In addition, the trend mainly falls in the

range of εNd_T commonly reported for mantle-derived rocks of the Superior Province (e.g., Machado et al., 1986; Polat and Kerrich, 2002; Tomlinson et al., 2004; Polat, 2009; Lodge et al., 2014). A plot of εNd_T against Eu/Eu* similarly shows that most samples cluster around 1 and that the more variable websteritic cumulates do not define any correlation between Eu anomalies and εNd_T values (Fig. 9c). A plot of $\varepsilon Nd_{T=2674Ma}$ versus LOI does not display any overall correlation for the Wawa xenoliths (Fig. 9d). If Group II samples are considered in isolation, then a positive trend is present for this Group, but only if the highest, and most suspect, εNd_T value is ignored. The case for a causal link in this trend is weakened by the fact that the two Wawa xenoliths with the most positive εNd_T values have intermediate LOI contents relative to the entire suite of Wawa xenoliths. In addition, the Group II LOI sub-trend can be related equally well to a positive εNd_T-MgO correlation (Fig. 9e) or negative εNd_T-REE and the susceptibility of more Mg-rich xenoliths to be affected by hydrous and/or CO_2-rich fluids in the mantle. As was the case for many element-element plots, Group III is distinct in showing a wide range of εNd_T compositions at relatively constant MgO. On a plot of εNd_T versus Ni contents, however, Groups I and II exhibit a positive correlation and Group III displays a negative correlation resulting in a "humped" distribution of εNd_T values over the total range of Ni (Fig. 9f).

It is difficult to envision a late alteration process, i.e. one acting on the emplaced lamprophyre and its xenoliths, which would produce the Ni-εNd_T relations observed in the Wawa xenoliths. The lamprophyres themselves have $\varepsilon Nd_{T=2674Ma}$ between 0 and +5

(Wyman et al., 2006). Therefore, we tentatively favour a syn-orogenic event acting on the Wawa subcontinental lithospheric mantle.

Based on the observations of Aulbach et al. (2013) for Slave Craton xenoliths, variable degrees of late Archean or early Proterozoic reworking eventually resulted in homogenization of the middle to lower SCLM, removing the highly variable εNd_T that are now only documented in shallow SCLM samples. The widespread "late tectonic" shoshonite-sanukitoid suite may well correspond to the initial phase of this homogenization process. Hydrothermal, critical or magmatic fluids associated with this event may have inherited the high εNd_T of garnets formed prior to orogeny (2900 Ma – 2700 Ma). For example, although garnets are typically LREE-MREE depleted versus their HREE, fluids calculated to be in equilibrium with majorite-bearing deep mantle lithologies display relative LREE enrichment (Fig. 5C; Kessel et al., 2005; Scambelluri et al., 2010). Moreover, progressive re-equilibration of garnet-bearing assemblages and the metasomatic recrystallization of early-formed garnets are well documented in the upper mantle (e.g., Griffin et al., 1984; Scambelluri et al., 2010) and could represent the source of the high εNd_T component observed in the Wawa xenoliths.

In this scenario, the positive correlations between MgO or Ni versus εNd_T shown by Groups I and II xenoliths reflects the general tendency of more mafic samples to have lower MREE contents, which results in greater shifts in εNd_T for a given amount of interaction with a high-εNd_T fluid or melt. In detail, the fluid – rock interaction on a uniform rock type such as the precursor Group 1A websterites described by Wyman et al.

(2006) would produce silica addition and a "local" negative correlation between MgO and εNd_T but among a diverse suite of precursor rocks, the overall trend would be a positive one.

The MgO systematics of the Group III xenoliths are clearly not attributable to typical igneous processes associated with a single magma. In a mixing process, however, it is possible that one component had a high εNd_T prior to the mixing event. Within the low-Nb Group III samples, it was the high-MgO but low-Ni sample that displays the highest εNd_T value (WX-10: $\varepsilon Nd_T = 10.2$).

Based on mantle xenolith studies word wide, it is possible that more that one metasomatic process is represented in the xenoliths (e.g., Downes et al., 2004; Franz and Romer, 2010). The two trends present on εNd_T vs Ce/Ce* or Eu/Eu* plots are consistent with two processes acting on the mantle regions represented by the xenoliths (Fig. 9). The sub-horizontal trends on the two plots are mainly defined by the websteritic rocks that Wyman et al. (2006) inferred were metasomatised by hydrous fluids enriched in LREE, but not the HFSE. The vertical trends on the two plots correspond to samples that display Zr-Hf enrichment along with the REE, but only minor or sporadic Nb enrichment. We infer that the trend corresponds to a metasomatic processes mediated by a critical fluid or small degree melt where rutile was generally present in the source.

5.3 Geodynamic Significance

The xenolith host rocks provide the first set of constraints on their geodynamic significance for orogeny in the southern Superior Province. For example, any "end member" model invoking formation of the deep cratonic keel by successive accretion of shallow dipping oceanic slabs appears to be unviable. The shoshonitic suite requires a strongly enriched (metasomatised) lithospheric, or perhaps asthenosphere wedge, as a source, which slab accretion models cannot account for. Wyman and Kerrich (2002, 2009) have discussed this issue in some detail in terms of the various post-plume volcanic rocks found in the southern Abitibi belt. For example, shallow mantle-derived mafic magmas were erupting late in the tectonic history of the Abitibi belt (Wyman and Hollings, 2006), implying that no keel was present shortly before orogeny or cratonization.

The Wawa xenoliths provide temporally well-constrained and direct evidence for components of the sub-greenstone belt mantle during a Late Archean orogeny that most researchers (e.g., Kimura et al., 1993; Ayer et al., 2002; Percival et al., 2012) agree followed a geodynamic history that involved both mantle plume and plate tectonic events. Tholeiitic signatures in least metasomatised websterites are suggested by low Nb/Zr ratios, where these could be measured, while the lowest εNd_T value of + 4 for these xenoliths (sample 97RPS0008 of Wyman et al., 2006) is consistent with values from mantle derived rocks from the southern Superior Province. Changing the age to T=2900 Ma shifts the εNd_T value of the sample to +1. Given that the + 4 value itself may correspond to some minor degree of metasomatic overprinting, it is not possible to establish which volcanic cycle the lower-Al websterites may be related to, based on the

Sm-Nd isotopic data. The fact that two distinct types of websterites are present in the xenolith suite in equal abundance suggests, however, that they are related to mafic magmatism in the 2.70 Ga Cycle 3 and (or) 2.75 Ga Cycle 2, which are more compositionally diverse than 2.90 Ga Cycle 1 basalts and include slightly LREE depleted and strongly LREE enriched varieties (Sylvester et al., 1986; Sage et al., 1996). The restriction of xenolith Pb isotopic results to the trend of post-2.9 Ga rocks in Figure 7B also supports this inference. In addition, the recent identification of a lamprophyre-hosted websteritic xenolith in the Abitibi belt with an $\varepsilon Nd_{T=2674Ma}$ value of +10.5 (A. Temelkovski, pers. comm., 2014) suggests that the presence of an older terrane was not required for the presence of these types of xenoliths or the metasomatic agents that acted on them.

A small proportion of Group II eclogitic xenoliths resemble the Group IB websterites in terms of their trace element distributions and may also be related to Cycle II and III magmatism. The great majority, however, display strong affinities with the host shoshonite suite and, as previously argued, are likely underplated counterparts to the volcanic and plutonic rocks. These interpretations for Group I and II xenoliths raise a key question about the source of metasomatic agent(s) observed in the Wawa xenoliths. If these are "sub arc" SCLM lithologies, then where was the source of the LREE-enriched and isotopically distinct fluids and melts that overprinted them? We cannot be entirely sure but based on the xenolith data, the characteristics of volcanism present in the three cycles, and geophysical data regarding the topography of base of the lithosphere, the following scenario appears plausible.

Based on the occurrence of 2.75 – 2.70 Ga cycles of non-plume volcanic rock types with arc-like affinities to the north of the 2.9 Ga sequences, and inboard of the hypothesized southern Superior subduction zone, the Wawa belt underwent ~ 2.72 Ga back arc rifting (Kerrich et al., 2008; Lodge et al., 2014), possibly in response to plume-arc interaction in the Abitibi sector of the arc (Fig. 10A). The ~2.9 Ga Hawk microcontinent was located on the trenchward side of the rift along with any keel retained from previous mantle plume activity. The Group I websterites represent cumulates from the later cycles of magmatism and were emplaced beneath the arc and backarc, and possibly within 2.9 Ga SCLM developed during the earlier mantle plume event. At around 2.69 Ga, the northern edge of Abitibi-Wawa arc amalgamated with the Superior Craton in what Percival et al. (2012) refer to as the Shebandowan Orogeny (Fig. 10B).. Based on Lithoprobe seismic imaging and magnetotelluric data (White et al., 2003; Craven et al., 2004; see Wyman, 2013), this northern suture appears to have involved "subcretion" of the slab onto the deep root of the Superior Province core. A large proportion of granitoids in the Abitibi-Wawa terrane were emplaced during this period and thickening of the arc root is likely to have occurred. The southern boundary of the accreted arc underwent a ~2.68 Ga Minnesotan orogeny (Fig. 10 C), involving the Minnesota River Valley and Pontiac terranes, which was associated with the emplacement of shoshonitic stocks and lamprophyres, the latter commonly containing diamonds.

Based on the presence of diamonds in shoshonitic magmas, Wyman et al. (2006, 2008) and O'Neill and Wyman (2006) argued that a variant of the "subduction diamond" model

(i.e., the diamonds retrieved from the mantle during subduction or shortly after) was required involving flat subduction prior to orogeny. Although the model may be considered "unconventional", the discovery of diamond in young lamprophyric rocks in the Japanese fore arc and the recurring association of alluvial diamonds in post-Archean "orogenic" gold districts that lack deep cratonic keels provides support for this hypothesis (Wyman et al., 2008; Wyman and Kerrich, 2009 and references therein). The new results for xenoliths in this study do not contradict this scenario and further emphasize a shallow mantle arc setting. In Figure 10B flat subduction is associated with buoyant komatiite-bearing hot spot or plateau sequences and the proximity of a mantle plume. The plume is distorted by subduction-driven mantle flow, despite its buoyancy, based on the recent experiments of Druken et al. (2014). Those experiments have not yet established the impact of the mantle plume on the subducting plate but any effect would likely contribute to slap flattening (e.g., Betts et al., 2015).

The modeling of normal and flat subduction by O'Neill and Wyman (2006) indicates that shallow subduction angles optimise the conditions required for a diamond-lamprophyre association. The P-T conditions associated with the shallow (~ 100km or less) diamond stability field only persist for a short period during orogeny and slab roll back or slab loss. The upwelling of mantle asthenosphere, possibly plume-related, is likely to drive a metasomatic front into the formerly isolated frozen or cooled wedge, which would promote the generation of K-rich magmas in the shallow mantle diamond stability window. This upwelling asthenosphere may convect deeply sourced diamonds into the wedge but there is a limit in the extent to which unmetasomatized mantle can participate

in the generation of the syn-orogenic K-rich magmas. Strongly depleted lithologies at the base of the deformed arc, however, would be subject to the incursion of fluids and melts, potentially resulting in local high-εNd_T signatures in Group I websterites.

Group II mafic xenoliths mainly correspond to underplated magmas and are dominated by samples with sanukitoid – shoshonite parentage. Although there are commonly mutual cross-cutting relationships between the lamprophyres and the syenitic stocks (Stott et al., 2002; Vaillancourt et al., 2005a), the dikes tend to be among the latest phases of the suite to be emplaced, allowing them to sample co-genetic magmas that had been underplated to the base of the arc or "intra-plated" within the older cumulate lithologies. Local partial melting of the sub-orogen mantle, resulting in variable chemical and isotopic modification of the shoshonitic magmas by melts with high LREE and Zr-Hf contents but low Nb-Ta, presumably due to the stability of rutile in the zones of melting.

Group III xenoliths were derived from similar depths and correspond to shoshonitic pyroxenite cumulates mixed with variably metasomatised SCLM. Abundant mafic enclaves or xenoliths in syenites and lamprophyres (Berger, 2006; Sage, 2000) indicate that mixing processes attributed to calc alkaline magmas beneath post-Archean continental arcs (e.g., Richards and Kerrich, 2007) likely occurred during emplacement of the shoshonite magmas. Although the orogenic event was much shorter in duration than an Andean-style melting, homogenization, storage and homogenization (MASH) event, the contemporaneous thickening and deformation of the sub-arc lithosphere may have reduced the distinction between crust and mantle "as differentiating intrusions crystallize

within peridotitic wall rocks, (and) ultramafic cumulates amass in lower-crustal magma chambers" (Hildreth and Moorbath, 1988, p. 483-484). In this setting, the stability of mantle diamond in the source region of shoshonite magmas would be short-lived once subduction ended (O'Neil and Wyman, 2006; Wyman et al., 2008). Diamond-bearing lamprophyres represent a late expression of the shoshonitic event and ascended rapidly through a zone of waning magma-SCLM mixing.

5.4 Regional Implications

The results of this study highlight an enigma that may be applicable to parts of other cratons. Xenoliths entrained in younger kimberlitic magmas provide evidence of Archean subcontinental lithospheric mantle beneath the study area and to the east (Kaminsky et al., 2002; Griffin et al., 2004), yet shoshonitic magmas and the ~ 2.70 Ga arc-type magmatism preclude the presence of a thick root prior to orogeny.

The comparatively shallow (~ 150 – 160 km) depths to the lithosphere – asthenosphere boundary along the southern Superior Province and its fertile nature have been interpreted by Faure et al. (2012) to be a feature that formed in the late Archean but was exploited by later geodynamic processes. Fertile Archean SCLM is most commonly accounted for by post-Archean replenishment during metasomatic events and this explanation likely applies to a large proportion of modified Archean keels worldwide (e.g., Griffin et al., 2009). The evidence provided by the Wawa xenoliths demonstrates that modification of the 2.9 Ga Hawk micro-continent keel may have begun in the

Archean, given the evidence for hydrous and magmatic fluids that were derived in part from a long-term depleted source. It is clear, however that the local reworking of a 2.9 Ga keel cannot account for a feature that extends along the entire southern margin of the craton.

Griffin et al. (2009) note that it is impossible to see through the metasomatic alteration that has affected many Archean keels and that focusing on the most depleted samples provides the best guide to the formation conditions during keel development. While this approach is entirely appropriate within the refertilized keel paradigm, it may overlook alternative or additional processes associated with keel formation. If keel – crust coupling is delayed until after orogeny due to intervening subducting slab, then later ascent of the plume residue is likely to involve a more heterogeneous mix of mantle components including fragments of oceanic slab and prevalent upper mantle. The process would likely not result in the inverted cone shape that characterizes intact keels generated by the unimpeded ascent of plume melt residues and would probably produce a locally thinner keel. An idealized representation in Figure 10D illustrates the re-establishment of an undisturbed plume underneath or outboard of the former trench. Depleted melt residue ascends in the trough area noted by Faure et al. (2012) and provides the cratonic root delineated by studies of post-Archean mantle xenoliths, but it will not be as thick as in regions of unimpeded plume ascent.

6 Conclusions

The xenoliths retrieved from lamprophyric hosts in the Michipicoten belt fall into a few well-defined groups, based on Al-Mg systematics, and do not include mantle peridotite. Based on immobile trace element contents, the xenoliths are derived from magmas associated with the main phase of arc volcanism between 2.75 and 2.70 Ga or are co-genetic with the shoshonite suite represented by syenitic intrusions and the host lamprophyres.

Trace elements distinguish two styles of metasomatism characterized either by LILE enrichment or both LILE and Zr-Hf enrichment and, less commonly, Nb-Ta. The first is likely associated with a hydrous fluid whereas the second is related to melts that permeated underplated shoshonitic mafic magmas and cumulates or the older sub-arc mantle. Although the significance of the two highest εNd_T values (> 20) are difficult to assess, the isotopic results overall indicate that an aged, highly depleted, source was tapped during the orogenic event. The most obvious source is the SCLM of the Hawk Terrane, but studies of post-Archean arcs indicate that suitable sources could readily exist within sub-arc lithologies generated 75 – 25 m.y. earlier.

The formation depths of the lamprophyric magmas, and the xenoliths they contain, contrast with the calculated depths to the base of the depleted lithosphere based on xenoliths retrieved from post-Archean kimberlites. The differences imply a late docking of the ~ 150-160 km deep Archean keel beneath the Abitibi-Wawa terrane. The results also imply that the geodynamic events responsible for an association of diamonds and

orogenic gold deposits in the southern Superior Province (Fig. 10c) are not linked to the presence of a deep sub-cratonic keel.

Acknowledgements

This research was funded by an NSERC Discovery grant to PH. Anne Hammond is thanked for thin-section preparation. The support for isotope analytical facilities and costs of Sm–Nd and Pb isotopic analyses were provided by LGI — Laboratório de Geologia Isotópica–UFRGS–Brazil. The comments of two reviewers genuinely helped us to clarify the text and improve the analysis of results.

References

Aulbach, S., Griffin, W.L., Pearson, N.J., O'Reilly, S.Y., 2013. Nature and timing of metasomatism in the stratified mantle lithosphere beneath the central Slave craton (Canada). Chemical Geology 352, 153-169.

Ayer, J.A., Thurston, P.C., Bateman, R., Dubé, B., Gibson, H.L., Hamilton, M.A., Hathway, B., Hocker, S.M., Houlé, M.G., Hudak, G., Ispolatov, V.O., Lafrance, B., Lesher, C.M., MacDonald, P.J., Péloquin, A.S., Piercey, S.J., Reed, L.E., Thompson, P.H., 2005. Overview of results from the Greenstone Architecture Project: Discover Abitibi Initiative; Ontario Geological Survey, Open File Report 6154, 146p.

Bailey, L.M., 1999. An unusual diamond-bearing talc schist from the Dachine area of French Guiana. Unpublished MSc thesis. Queen's University, Canada, p. 161.

Barth, M.G., Rudnick, R.L., Horn, I., McDonough, W.F., Spicuzza, M.J., Valley, J.W., Haggerty, S.E., 2001. Geochemistry of xenolithic eclogites from West Africa, part I: A link between low MgO eclogites and Archean crust formation. Geochimica et Cosmochimica Acta 65, 1499-1527.

Barth, M.G., Rudnick, R.L., Horn, I., McDonough, W.F., Spicuzza, M.J., Valley, J.W., Haggerty, S.E., 2002. Geochemistry of xenolithic eclogites from West Africa, part 2: Origins of the high MgO eclogites. Geochimica et Cosmochimica Acta 66, 4325-4345.

Bédard, J.H., Harris, L.B., 2014. Neoarchean disaggregation and reassembly of the Superior craton. Geology 42, 951-954.

Berger, B.R., 2006. Geological synthesis along Highway 66 from Matachewan to Swastika; Ontario Geological Survey, Open File Report 6177, 125p.

Berly, T.J., Hermann, J., Arculus, R.J., Lapierre, H., 2006. Supra-subduction Zone Pyroxenites from San Jorge and Santa Isabel (Solomon Islands). Journal of Petrology 47, 1531-1555.

Betts, P.G., Moresi, L., Miller, M.S., Willis, D., 2015. Geodynamics of oceanic plateau and plume head accretion and their role in Phanerozoic orogenic systems of China. Geoscience Frontiers 6, 49-59.

Bodinier, J.-L., Garrido, C.J., Chanefo, I., Bruguier, O., Gervilla, F., 2008. Origin of Pyroxenite–Peridotite Veined Mantle by Refertilization Reactions: Evidence from the Ronda Peridotite (Southern Spain). Journal of Petrology 49, 999-1025.

Bodinier, J.L., Godard, M., 2003. Orogenic, Ophiolitic and Abyssal Peridotites. , in: Carlson, R.W. (Ed.), Treatise on Geochemistry, Mantle and Core. Volume 2. Elsevier, pp. 103-170.

Burnham, O.M., and Schweyer, J. 2004. Trace Element Analysis of Geological Samples by ICP-MS at the Geoscience Laboratories: Revised Capabilities Due to Improvements to Instrumentation. *In* Summary of Field Work and Other Activities 2004. Ontario Geological Survey Open File Report 6145, 54-1 to 54-20.

Burnham, O.M., Hechler, J.H., Semenyna, L., and Schweyer, J. 2002. Mineralogical controls on the determination of trace elements following mixed acid dissolution. *In* Summary of Field Work and Other Activities 2002. Ontario Geological Survey Open File Report 6100, 36-1 to 36-12.

Calvert, A.J., Sawyer, E.W., Davis, W.J., Ludden, J.N., 1995. Archaean subduction inferred from seismic images of a mantle suture in the Superior Province. Nature 375, 670-674.

Capdevila, R., Arndt, N., Letendre, J., Sauvage, J.-F., 1999. Diamonds in volcaniclastic komatiite from French Guiana. Nature 399, 456-458.

Card, K.D., Ciesielski, A., 1986. DNAG#1, Subdivisions of the Superior Province of the Canadian Shield. Geoscience Canada 13, 5-13.

Carignan, J., Gariépy, C., Machado, N., Rive, M., 1993. Pb isotopic geochemistry of granitoids and gneisses from the late Archean Pontiac and Abitibi Subprovinces of Canada. Chemical Geology 106, 299-315.

Corfu, F., Sage, R.P., 1992. U–Pb age constraints for deposition of clastic metasedimentary rocks and late-tectonic plutonism, Michipicoten Belt, Superior Province. Canadian Journal of Earth Sciences 29, 1640-1651.

De Stefano, A., Lefebvre, N., Kopylova, M., 2006. Enigmatic diamonds in Archean calc-alkaline lamprophyres of Wawa, southern Ontario, Canada. Contributions to Mineralogy and Petrology 151, 158-173.

der Wal, D.V., Bodinier, J.L., 1996. Origin of the recrystallisation front in the Ronda peridotite by km-scale pervasive porous melt flow. Contributions to Mineralogy and Petrology 122, 387-405.

Dostal, J., Mueller, W.U., 1997. Komatiite Flooding of a Rifted Archean Rhyolitic Arc Complex: Geochemical Signature and Tectonic Significance of the Stoughton- Roquemaure Group, Abitibi Greenstone Belt, Canada. The Journal of Geology 105, 545-564.

Dostal, J., Mueller, W.U., 2013. Deciphering an Archean mantle plume: Abitibi greenstone belt, Canada. Gondwana Research 23 (2013) 493-505.

Downes, H., Macdonald, R.A.Y., Upton, B.G.J., Cox, K.G., Bodinier, J.-L., Mason, P.R.D., James, D., Hill, P.G., Hearn, B.C., 2004. Ultramafic Xenoliths from the Bearpaw Mountains, Montana, USA: Evidence for Multiple Metasomatic Events in the Lithospheric Mantle beneath the Wyoming Craton. Journal of Petrology 45, 1631-1662.

Faure, S., Godey, S., Fallara, F., Trepanier, S., 2011. Seismic Architecture of the Archean North American Mantle and Its Relationship to Diamondiferous Kimberlite Fields. Economic Geology 106, 223-240.

Franz, L., Romer, R.L., 2010. Different styles of metasomatic veining in ultramafic xenoliths from the TUBAF Seamount (Bismarck Microplate, Papua New Guinea). Lithos 114, 30-53.

Gariépy, C., Allégre, C.J., Lajoie, J., 1984. U-Pb systemstics in single zircons from the Pontiac sediments, Abitibi greenstone belt. Canadian Journal of Earth Sciences 21, 1296-1304.

Garrido, C.J., Bodinier, J.-L., 1999. Diversity of Mafic Rocks in the Ronda Peridotite: Evidence for Pervasive Melt–Rock Reaction during Heating of Subcontinental Lithosphere by Upwelling Asthenosphere. Journal of Petrology 40, 729-754.

Gonzaga, R.G., Lowry, D., Jacob, D.E., LeRoex, A., Schulze, D., Menzies, M.A., 2010. Eclogites and garnet pyroxenites: Similarities and differences. Journal of Volcanology and Geothermal Research 190, 235-247.

Grabowski, G.P.B., Wilson, A.C., 2005. Sampling lamprophyre dikes for diamonds: Discover Abitibi Initiative; Ontario Geological Survey, Open File Report 6170, 262p.

Griffin, W.L., O'Reilly, S.Y., 2007. Cratonic lithospheric mantle: Is anything subducted? Episodes 30, 43-53.

Griffin, W.L., O'Reilly, S.Y., Afonso, J.C., Begg, G.C., 2009. The composition and evolution of lithospheric mantle: A re-evaluation and its tectonic implications. Journal of Petrology 50, 1185-1204.

Griffin, W.L., O'Reilly, S.Y., Doyle, B.J., Pearson, N.J., Coopersmith, H., Kivi, K., Malkovets, V., Pokhilenko, N., 2004. Lithosphere mapping beneath the North American plate. Lithos 77, 873-922.

Griffin, W.L., O'Reilly, S.Y., Ryan, C.G., Gaul, O., Ionov, D.A., 1998. Secular Variation in the Composition of Subcontinental Lithospheric Mantle: Geophysical and Geodynamic Implications, Structure and Evolution of the Australian Continent. American Geophysical Union, pp. 1-26.

Griffin, W.L., Wass, S.Y., Hollis, J.D., 1984. Ultramafic xenoliths from Bullenmerri and Gnotuk Maars, Victoria, Australia: Petrology of a sub-continental crust-mantle transition. Journal of Petrology 25, 53-87.

Helmstaedt, H.H., Gurney, J.J., Richardson, S.H., 2010. Ages of Cratonic Diamonds and Lithosphere evolution: constraints on Precambrian tectonics and diamond exploration. The Canadian Mineralogist 48, 1385-1408.

Hildreth, W., Moorbath, S., 1988. Crustal contributions to arc magmatism in the Andes of Central Chile. Contributions to Mineralogy and Petrology 98, 455-489.

Hollings, P., Wyman, D., 1999. Trace element and Sm-Nd systematics of volcanic and intrusive rocks from the 3 Ga Lumby Lake Greenstone belt, Superior Province: Evidence for Archean plume-arc interaction. Lithos 46, 189-213.

Jacob, D.E., 2004. Nature and origin of eclogite xenoliths from kimberlites. Lithos 77, 295-316.

Kaminsky, F.V., Sablukov, S.M., Sablukova, L.I., Shchukin, V.S., Canil, D., 2002. Kimberlites from the Wawa area, Ontario. Canadian Journal of Earth Sciences 39, 1819-1838.

Kessel, R., Schmidt, M.W., Ulmer, P., Pettke, T., 2005. Trace element signature of subduction-zone fluids, melts and supercritical liquids at 120-180[thinsp]km depth. Nature 437, 724-727.

Ketchum, J.W.F., Ayer, J.A., Van Breemen, O., Pearson, N.J., Becker, J.K., 2008. Pericontinental crustal growth of the southwestern abitibi subprovince, Canada - U-Pb, Hf, and Nd isotope evidence. Economic Geology 103, 1151-1184.

Kimura, G., Ludden, J.N., Desrochers, J.P., Hori, R., 1993. A model of ocean-crust accretion for the Superior province, Canada. Lithos 30, 337-355.

Kopylova, M.G., Afanasiev, V.P., Bruce, L.F., Thurston, P.C., Ryder, J., 2011. Metaconglomerate preserves evidence for kimberlite, diamondiferous root and medium grade terrane of a pre-2.70 Ga Southern Superior protocraton. Earth and Planetary Science Letters 312, 213-225.

Krogh, T.E., Turek, A., 1982. Precise U–Pb zircon ages from the Gamitagama greenstone belt, southern Superior Province. Canadian Journal of Earth Sciences 19, 859-867.

Lefebvre, N., Kopylova, M., Kivi, K., 2005. Archean calc-alkaline lamprophyres of Wawa, Ontario, Canada: Unconventional diamondiferous volcaniclastic rocks. Precambrian Research 138, 57-87.

Lodge, R.W.D., Gibson, H.L., Stott, G.M., Franklin, J.M., Hamilton, M.A., 2014. Geodynamic Reconstruction of the Winston Lake Greenstone Belt and VMS Deposits: New Trace Element Geochemistry and U-Pb Geochronology. Economic Geology 109, 1291-1313.

Machado, N., Brooks, C., Hart, S.R., 1986. Determination of initial and in primary minerals from mafic and ultramafic rocks: Experimental procedure and implications for the isotopic characteristics of the Archean mantle under the Abitibi greenstone belt, Canada. Geochimica et Cosmochimica Acta 50, 2335-2348.

Marchesi, C., Garrido, C.J., Bosch, D., Bodinier, J.-L., Gervilla, F., Hidas, K., 2013. Mantle refertilization by melts of crustal-derived garnet pyroxenite: Evidence from the Ronda peridotite massif, southern Spain. Earth and Planetary Science Letters 362, 66-75.

McCuaig, T.C., Kerrich, R., and Xie, Q. 1994. Phosphorous and high field strength anomalies in Archean high-magnesian magmas as possible indicators of source mineralogy and depth. Earth and Planetary Science Letters, 124, 221-239.

McDonough, W.F., Sun, S.S., 1995. The composition of the Earth. Chemical Geology 120 223-253.

Mole, D.R., Fiorentini, M.L., Thebaud, N., Cassidy, K.F., McCuaig, T.C., Kirkland, C.L., Romano, S.S., Doublier, M.P., Belousova, E.A., Barnes, S.J., Miller, J., 2014. Archean komatiite volcanism controlled by the evolution of early continents. Proceedings of the National Academy of Sciences. www.pnas.org/cgi/doi/10.1073/pnas.1400273111

Moser, D.E., 1994. The geology and structure of the mid-crustal Wawa gneiss domain: a key to understanding tectonic variation with depth and time in the late Archean Abitibi–Wawa orogen. Canadian Journal of Earth Sciences 31, 1064-1080.

O'Neill, C., Wyman, D.A., 2006. Geodynamic Modeling of Late Archean Subduction: Pressure-Temperature Constraints from Greenstone Belt Diamond Deposits, Archean Geodynamics and Environments. American Geophysical Union, pp. 177-188.

Percival, J.A., Skulski, T., Sanborn-Barrie, M., Stott, G.M., Leclair, A.D., Corkery, M.T., Boily, M., 2012. Geology and Tectonic Evolution of the Superior Province, Canada in: Percival, J.A., Cook, F.A., Clowes, R.M. (Eds.), Tectonic Styles in Canada: The LITHOPROBE Perspective. Geological Association of Canada Special Paper 49, pp. 321-378.

Pearson, D.G., Canil, D., Shirey, S.B., 2003. Mantle Samples Included in Volcanic Rocks: Xenoliths and Diamonds, in: Carlson, R.W. (Ed.), Treatise on Geochemistry, Volume 2. Elsevier, pp. 171-275.

Pearson, D.G., Shirey, S.B., Carlson, R.W., Boyd, F.R., Pokhilenko, N.P., Shimizu, N., 1995. Re-Os, Sm-Nd, and Rb-Sr isotope evidence for thick Archaean lithospheric mantle beneath the Siberian craton modified by multistage metasomatism. Geochimica et Cosmochimica Acta 59, 959-977.

Polat, A., 2009. The geochemistry of Neoarchean (ca. 2700 Ma) tholeiitic basalts, transitional to alkaline basalts, and gabbros, Wawa Subprovince, Canada: Implications for petrogenetic and geodynamic processes. Precambrian Research 168, 83-105.

Polat, A., Kerrich, R., 2002. Nd-isotope systematics of ~2.7 Ga adakites, magnesian andesites, and arc basalts, Superior Province: evidence for shallow crustal recycling at Archean subduction zones. Earth and Planetary Science Letters 202, 345-360.

Polat, A., Kerrich, R., Wyman, D.A., 1998. The late Archean Schreiber, Hemlo and White River, Dayohessarah greenstone belts, Superior Province: collages of oceanic plateaus, oceanic arcs, and subduction, accretion complexes. Tectonophysics 289, 295-326.

Polat, A., Kerrich, R., Wyman, D.A., 1999. Geochemical diversity in oceanic komatiites and basalts from the late Archean Wawa greenstone belts, Superior Province, Canada: Trace element and Nd isotope evidence for a heterogeneous mantle. Precambrian Research 94, 139-173.

Rayner, N., Stott, G.M., 2005. Discrimination of Archean domains in the Sachigo Subprovince: a progress report on the geochronology. In: Baker, C.L., Debicki, E.J., Kelly, R.I., Ayer, J.A., Easton, R.M., Madon, Z.B. (Eds.), Summary of Field Work and Other Activities 2005. Ontario Geological Survey, Open File Report 6172, pp. 10-1–10-21.

Rice, R.J., Donaldson, J.A., 1992. Sedimentology of the Archean Doré metasediments, Arliss Lake area, southern Michipicoten greenstone belt, Superior Province. Canadian Journal of Earth Sciences 29, 2558-2570.

Richards, J.P., Kerrich, R., 2007. Adakite-like rocks: Their diverse origins and questionable role in metallogenesis. Economic Geology 102, 537-576.

Sage, R.P., 1994. Precambrian geology, Michipicoten Greenstone Belt, central portion; Ontario Geological Survey, Preliminary Map P.3303, scale 1:50 000.

Sage, R.P., 2000. The "Sandor" Diamond Occurrecne, Michipicoten Greenstone Belt, Wawa, Ontario: A Preliminary Study; Ontario Geological Survey, Open File Report 6016, 49p.

Sage, R.P., Lightfoot, P.C., Doherty, W., 1996a. Bimodal cyclical Archean basalts and rhyolites from the Michipicoten (Wawa) greenstone belt, Ontario: geochemical evidence for magma contributions from the asthenospheric mantle and ancient continental lithosphere near the southern margin of the Superior Province. Precambrian Research 76, 119-153.

Sage, R.P., Lightfoot, P.C., Doherty, W., 1996b. Geochemical characteristics of granitoid rocks from within the Archean Michipicoten Greenstone Belt, Wawa Subprovince, Superior Province, Canada: implications for source regions and tectonic evolution. Precambrian Research 76, 155-190.

Scambelluri, M., Van Roermund, H.L.M., Pettke, T., 2010. Mantle wedge peridotites: Fossil reservoirs of deep subduction zone processes: Inferences from high and ultrahigh-pressure rocks from Bardane (Western Norway) and Ulten (Italian Alps). Lithos 120, 186-201.

Schiano, P., Monzier, M., Eissen, J.P., Martin, H., Koga, K., 2010. Simple mixing as the major control of the evolution of volcanic suites in the Ecuadorian Andes. Contributions to Mineralogy and Petrology 160, 297-312.

Scully, K.R., Canil, D., Schulze, D.J., 2004. The lithospheric mantle of the Archean Superior Province as imaged by garnet xenocryst geochemistry. Chemical Geology 207, 189-221.

Shirey, S.B., Hanson, G.N., 1984. Mantle-derived Archaean monozodiorites and trachyandesites. Nature 310, 222-224.

Stachel, T., Banas, A., Muehlenbachs, K., Kurszlaukis, S., Walker, E.C., 2006. Archean diamonds from Wawa (Canada): samples from deep cratonic roots predating cratonization of the Superior Province. Contributions to Mineralogy and Petrology 151, 737-750.

Stott, G.M., Ayer, J.A., Wilson, A.C., Grabowski, G.P.B., 2002. Are the Neoarchean diamond-bearing breccias in the Wawa area related to late-orogenic alkalic and "sanukitoid" intrusions? Summary of Field Work and Other Activities 2002, Ontario Geological Survey, Open File Report 6100, 9-1 –9-10., Open File Report 6100, pp. 9-1 –9-10.

Stott, G.M., Corkery, M.T., Percival, J.A., Simard, M., Goutier, J., 2010. A revised terrane subdivision of the Superior Province. In: Ayer, J.A., Easton, R.M., Beakhouse, G.P., Stott, G.M., Kelly, R.I., Debicki, E.J., Parker, J.R., Brown, T. (Eds.), Summary of Field Work and Other Activities 2010. Ontario Geological Survey, Open File Report 6260, pp. 20-1–20-10.

Sun, S.s., McDonough, W.F., 1989. Chemical and isotopic systematics of oceanic basalts: implications for mantle composition and processes. Geological Society, London, Special Publication 42, 313-345.

Sylvester, P.J., Attoh, K., Schulz, K.J., 1987. Tectonic setting of late Archean bimodal volcanism in the Michipicoten (Wawa) greenstone belt, Ontario. Canadian Journal of Earth Sciences 24, 1120-1134.

Thorpe, R.I., 2008. Release of lead isotope data in 4 databases: Canadian, Western Superior, foreign, and whole rock and feldspar. Geological Survey of Canada Open File 5664.

Thorpe, R.I., Sage, R.P., Franklin, J.M., 1987. Lead isotope evidence for an old crustal source for many ore leads in the Wawa region, Institute on Lake Superior Geology, Proceedings and Abstracts, pp. 76-77.

Thurston, P.C., Kamber, B.S., Whitehouse, M., 2012. Archean cherts in banded iron formation: Insight into Neoarchean ocean chemistry and depositional processes. Precambrian Research 214–215, 227-257.

Tomlinson, K.Y., Bowins, R., and Heshler, J. 1998. Refinement of Hafnium (Hf) and Zirconium (Zr) analysis by improvement in the sample digestion procedure. Ontario Geological Survey, Miscellaneous Paper 169, 189–192.

Tomlinson, K.Y., Stott, G.M., Percival, J.A., Stone, D., 2004. Basement terrane correlations and crustal recycling in the western Superior Province: Nd isotopic character of granitoid and felsic volcanic rocks in the Wabigoon subprovince, N. Ontario, Canada. Precambrian Research 132, 245-274.

Vaillancourt, C., Ayer, J.A., Hamilton, M.A., 2005a. Project Unit 03-002. Synthesis of Archean Geology and Diamond-bearing Rocks in the Michipicoten Greenstone Belt: Results from Microdiamond Extraction and Geochronological Analyses, pp. 8-1 to 8-13.

Vaillancourt, C., Dessureau, G.R., Zubowski, S.M., 2005b. Precambrian geology of Menzies Township; Ontario Geological Survey, Preliminary Map P.3366, scale 1:20 000.

van der Meer, Q.H.A., Klaver, M., Waight, T.E., Davies, G.R., 2013. The provenance of sub-cratonic mantle beneath the Limpopo Mobile Belt (South Africa). Lithos 170–171, 90-104.

Varfalvy, V., Hebert, R., Bedard, J.H., Lafleche, M.R., 1997. Petrology and geochemistry of pyroxenite dykes in upper mantle peridotites of the North Arm Mountain Massif, Bay of Islands Ophiolite, Newfoundland; implications for the genesis of boninitic and related magmas. The Canadian Mineralogist 35, 543-570.

Wendland, C., Fralick, P., Hollings, P., 2012. Diamondiferous, Neoarchean fan-delta deposits, western Superior Province, Canada: Sedimentology and provenance. Precambrian Research 196–197, 46-60.

Williams, H.R., Stott, G.M., B., H.K., L., M.T., Sage, R.P., 1991. Wawa Subprovince, Geology of Ontario, Ontario Geological Survey, Special Volume 4, Part 1, pp. 485-539.

Wilson, A., 2005 Ontario Ministry of Northern Development and Mines Mineral Deposit Identification File MDI42C02NW00026: Deposit Name MEN-107. http://www.geologyontario.mndmf.gov.on.ca/gosportal/gos?command=mndmsearchdetails:mdi&uuid=MDI42C02NW00026 Accessed July 9, 2014.

Wyman, D.A., 2013. A critical assessment of neoarchean "plume only" geodynamics: Evidence from the superior province. Precambrian Research 229, 3-19.

Wyman, D.A., Ayer, J.A., Conceição, R.V., Sage, R.P., 2006. Mantle processes in an Archean orogen: Evidence from 2.67 Ga diamond-bearing lamprophyres and xenoliths. Lithos 89, 300-328.

Wyman, D.A., Hollings, P., 2006. Late Archean convergent margin volcanism in the Superior Province: A comparison of the Blake River Group and Confederation Assemblage, in: Benn, K., Mareschal, J.-C., Condie, K. (Eds.), American Geophysical Union Monograph 164, Archean Geodynamics and Environments, pp. 215 – 238.

Wyman, D.A., Kerrich, R., 1989. Archean lamprophyre dikes of the Superior Province, Canada: distribution, petrology, and geochemical characteristics. Journal of Geophysical Research 94, 4667-4696.

Wyman, D.A., Kerrich, R., 1993. Archean Shoshonitic Lamprophyres of the Abitibi Subprovince, Canada: Petrogenesis, Age, and Tectonic Setting. Journal of Petrology 34, 1067-1109.

Wyman, D., Kerrich, R., 2009. Plume and arc magmatism in the Abitibi subprovince: Implications for the origin of Archean continental lithospheric mantle. Precambrian Research 168, 4-22.

Wyman, D.A., Kerrich, R., Polat, A., 2002. Assembly of Archean cratonic mantle lithosphere and crust: Plume-arc interaction in the Abitibi-Wawa subduction-accretion complex. Precambrian Research 115, 37-62.

Wyman, D.A., O'Neill, C., Ayer, J.A., 2008. Evidence for Modern-Style Subduction to 3.1 Ga: A Plateau – Adakite – Gold (Diamond) Association, in: Condie, K.C., Pease, V. (Eds.), When Did Plate Tectonics Begin on Planet Earth? GSA Special Paper 440. Geological Society of America, pp. 129-148.

Figure Captions

Figure 1. A) Location of the Superior Province Craton. B) Terranes of the Superior Province Craton, showing location of C) the study area in the Michipicoten greenstone belt. Adapted from Rayner and Stott (2005), Stott et al. (2010), Vaillancourt et al. (2005b) and Lefebvre et al. (2005).

Figure 2. A) Compositional overlap between diamondiferous Wawa breccia samples O2DS-86 and -87 (Wyman et al., 2006) and Dachine diamond host rocks (Wyman et al., 2008). B) Comparison of Dachine garnets (grey circles) from Bailey (1999) and Wawa garnet analyses (squares) reported by Kopylova et al. (2011). C) Dachine Mg-ilmenites compared with picro-ilmenite data from bulk sampling of the Wawa Leadbetter conglomerate. Field corresponds to kimberlite picroilmenites for S. Africa, S. America and N. America (Wyatt et al., 2004). Panels B and C adapted from Kopylova et al. (2011) and data sources therein.

Figure 3. Major element variation diagrams for the Wawa xenolith Groups distinguished according to MgO (Mg#) – Al_2O_3 characteristics (see text). IIIa= Group III data from Wyman et al. (2006). Data for lamprophyres and syenites from Wyman and Kerrich (1989) and Wyman et al. (2006). Bearpaw xenolith data from Downes et al (2004), Ronda data from Der Wal and Bodinier (1996). Dash line fields in B are from Berly et al. (2006). Numbered fields are Ronda Massif from Garrido and Bodinier (1999): 1=mafic garnet granulite; 2=garnet clinopyroxenite, websterite; 3= spinel websterite, intermediate

Ti-number; 4= spinel websterite, high Ti-number; 5 = spinel olivine websterite; 6= low Ti-number websterite, spinel websterite and orthopyroxenite.

Figure 4. Compatible element systematics of the Wawa xenoliths. See Figure 3 for symbol legend and other data sources.

Figure 5. Primitive mantle normalized multielement plots for xenolith Groups 1-4. Shaded area: Group IA websterites from Wyman et al. (2006). Fluid in equilibrium with composition shown in panel C derived from Scambelluri et al.'s (2010) sample M3-3 and Kessel et al.'s (2005) 6 Gpa garnet + fluid compositions. Primitive mantle normalizing factors from McDonough and Sun (1995).

Figure 6. Nb/Nb* versus Al_2O_3 wt.%. See Figure 3 for symbol legend and other data sources.

Figure 7. A) Sm-Nd and B) Pb-Pb isotope systematics of the Wawa xenoliths. Wyman et al. (2006) provide an expanded plot of the εNd_T versus Nd trend for Group IA samples. Data in B) for Wawa belt ore deposits from Thorpe et al. (1987) and for Wawa Cycle 1 and 2 rocks from Thorpe (2008). See Figure 3 for other symbols and data sources.

Figure 8. Th/Nd vs Th at two scales along the x axis. Line shows trend of low-Nb Group III samples. Two high-Nb Group III samples are noted. See Figure 3 for symbol legend and other data sources.

Figure 9. εNd_T versus major and trace element abundances, plus LOI. See text for discussion. See Figure 3 for symbol legend and other data sources.

Figure 10. Geodynamic evolution of the western Wawa-Abitibi Terrane showing a scenario to account for entrainment of sub-arc xenoliths in Archean lamprophyres and post-Archean entrainment of more typical depleted Archean cratonic root in kimberlites. A) 2.72 Ga Ma rifting the Wawa with embedded Hawk Terrane. B) ~ 2.72 Ga mantle plume ascent and slab-related mantle flow distortion (Druken et al., 2014), including hot core and restite (darker grey), followed by plateau/hotspot subduction, flat subduction and northern 2.69 Ga Shebandowan Orogeny. C) 2.68 Ga Minnesotan Orogen, slab roll back-slab loss and reheating of previously isolated and frozen wedge leading to shoshonitic magmatism, contemporaneous gold mineralization and the rapid loss of "subduction diamond" stability (Wyman et al., 2006, 2008). D) Rise of buoyant plume restite and amalgamation of greenstone crust and shallow lithospheric mantle with characteristic Archean depleted keel.

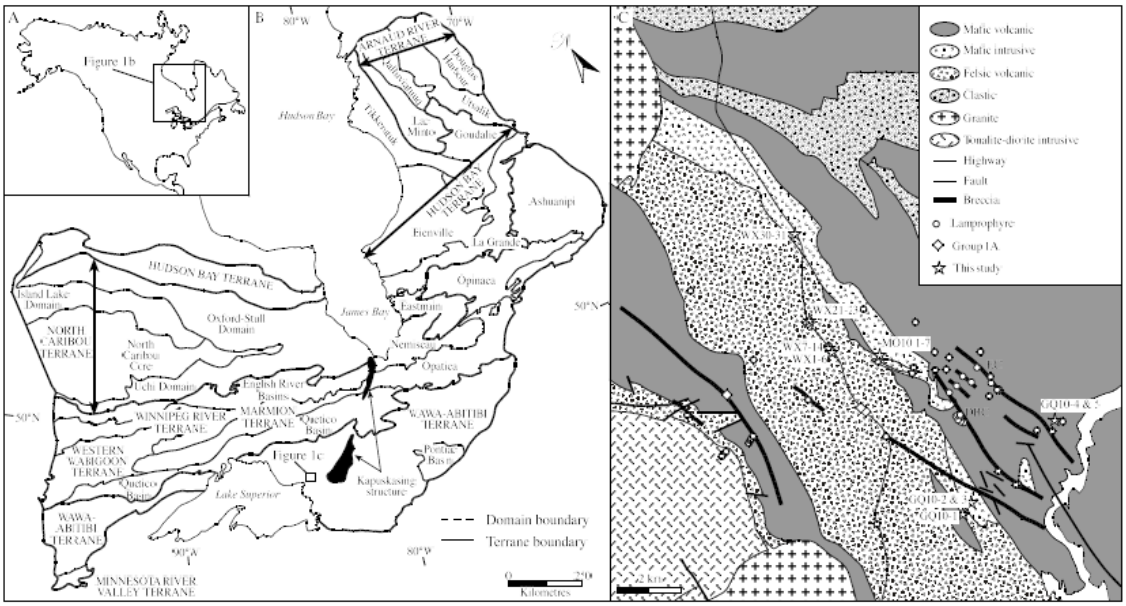

Figure 1

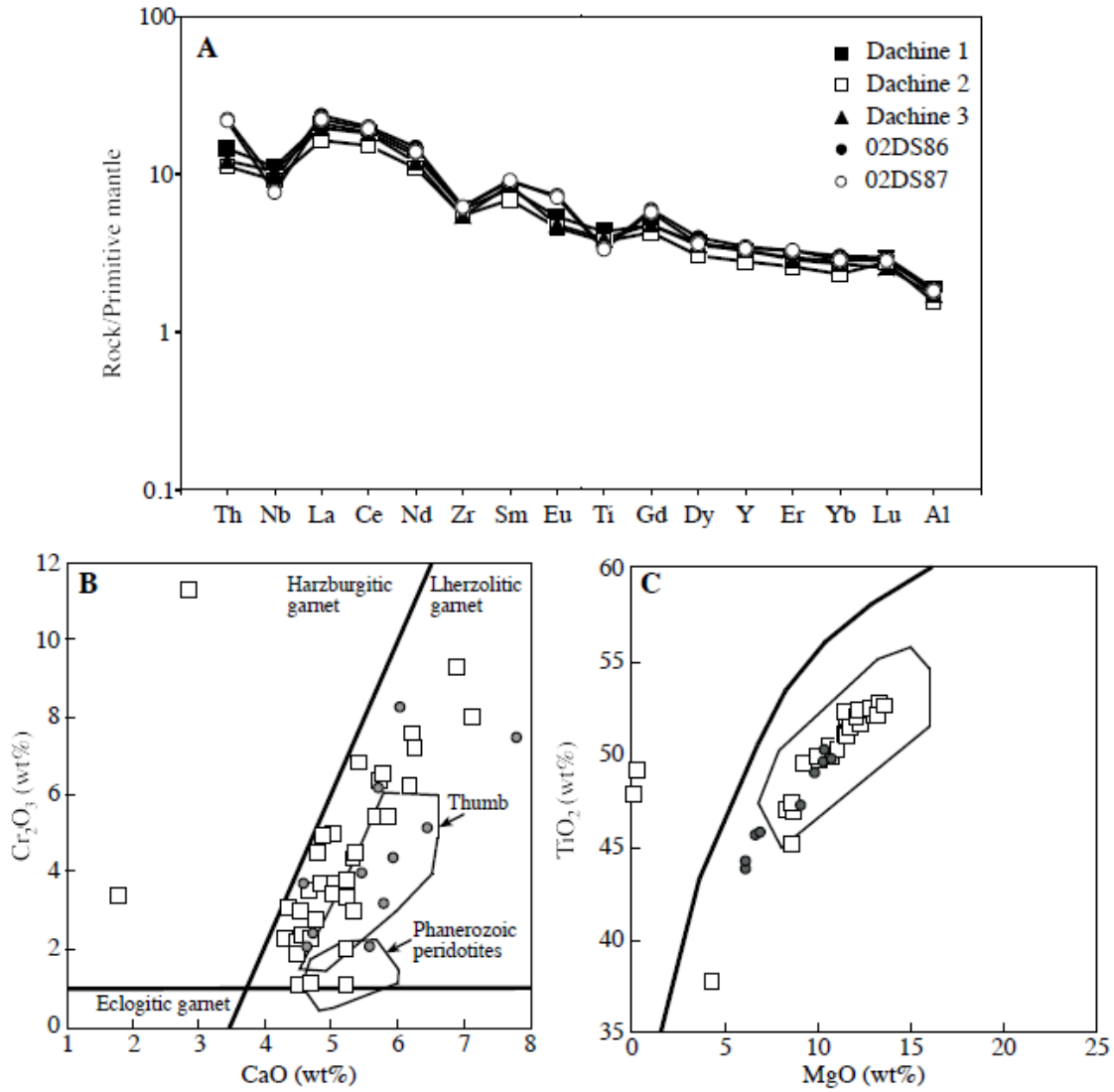

Figure 2

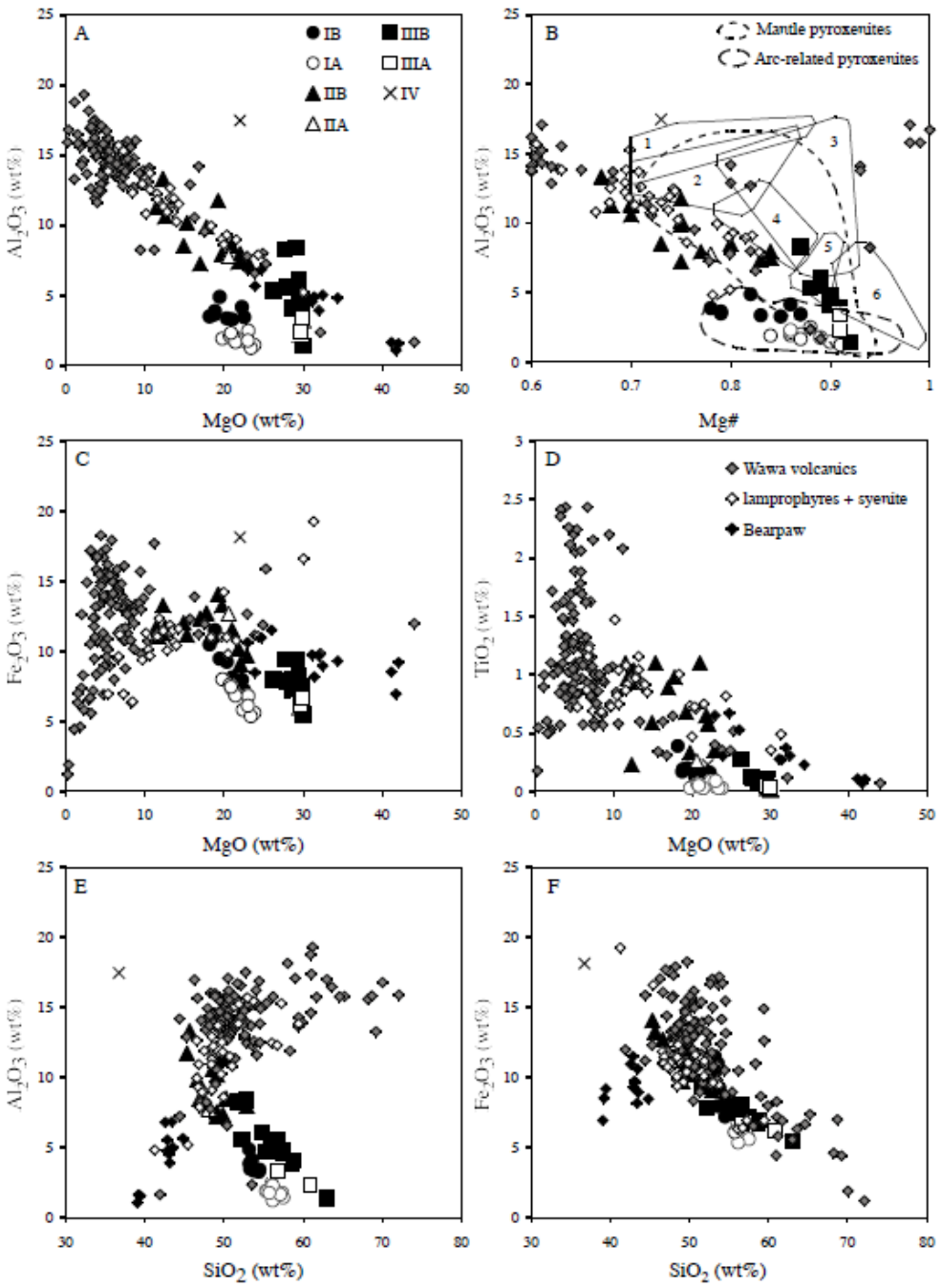

Wyman et al., Figure 3

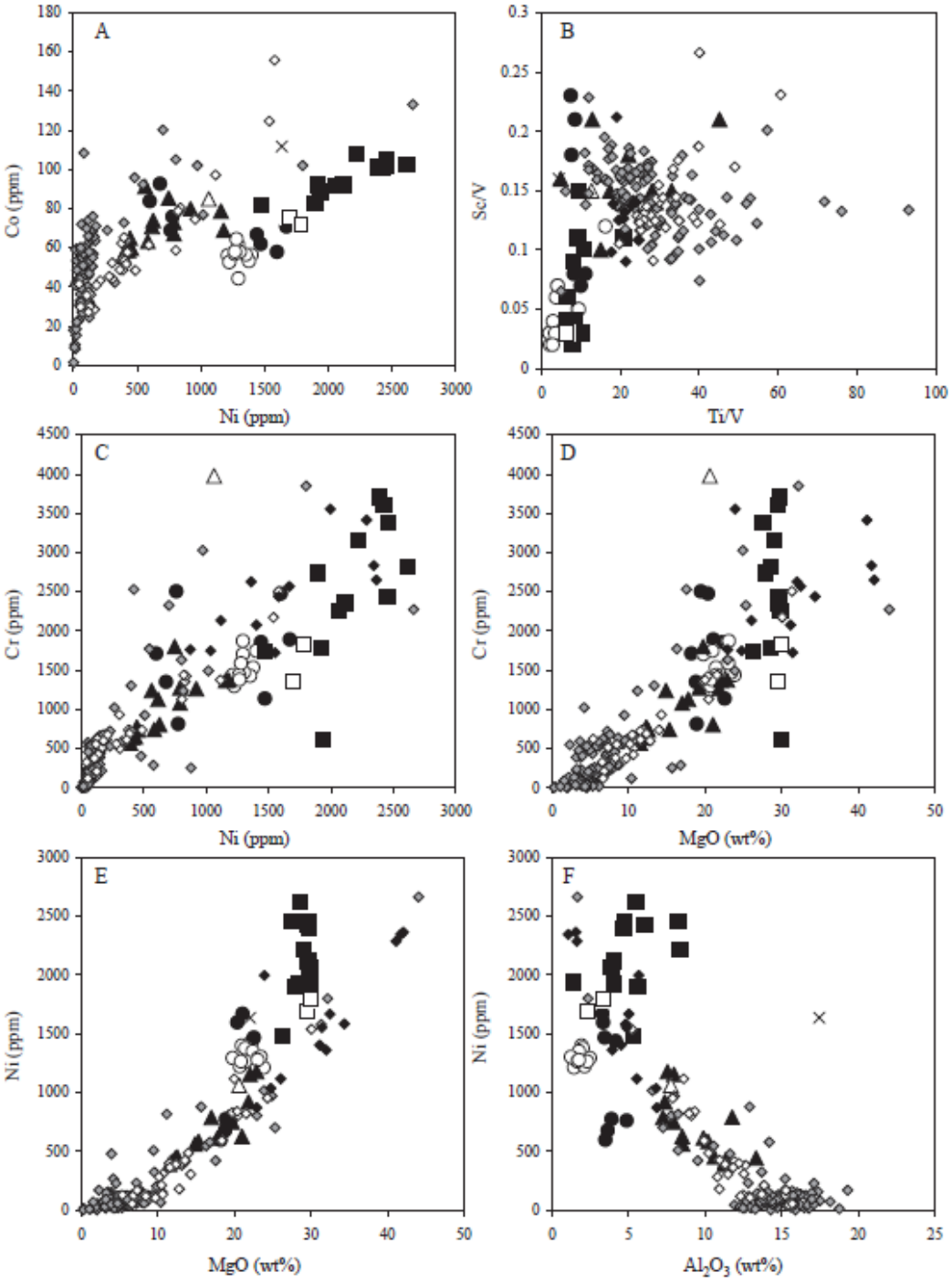

Wyman et al., Figure 4

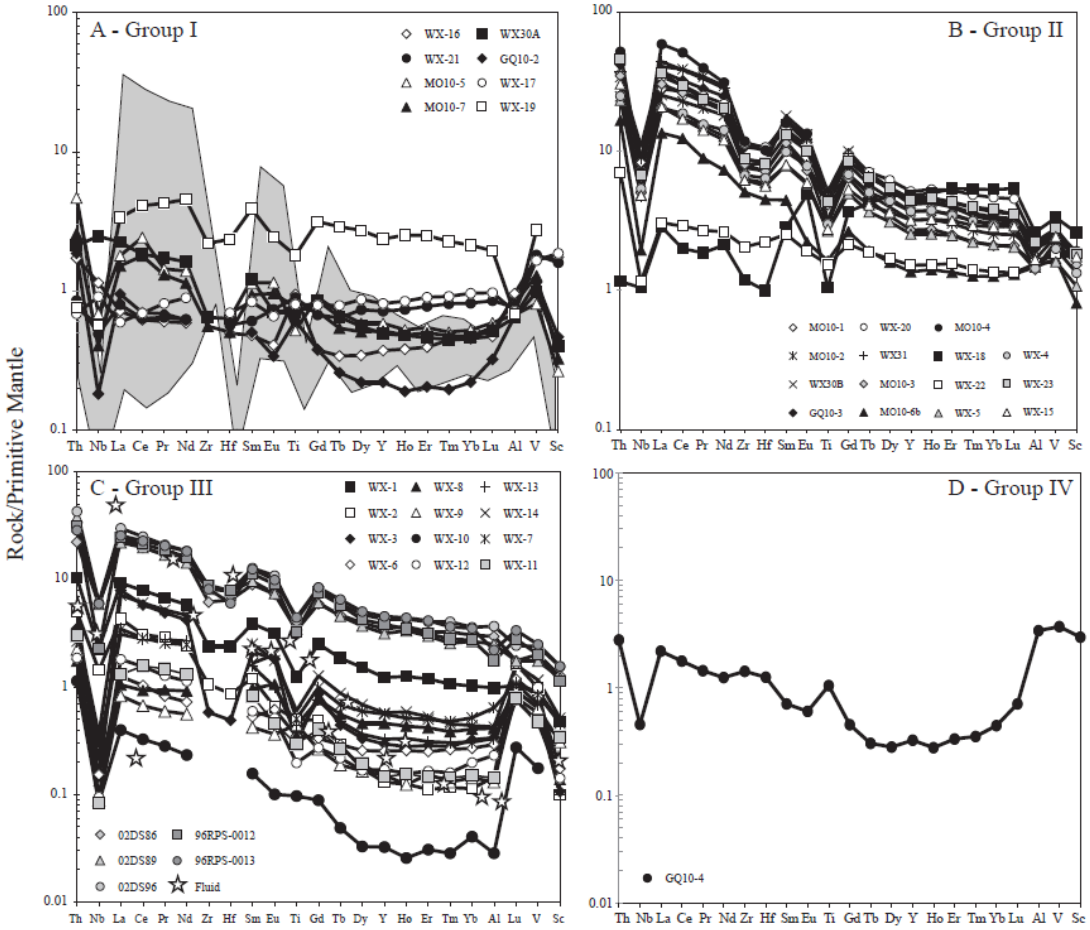

Figure 5

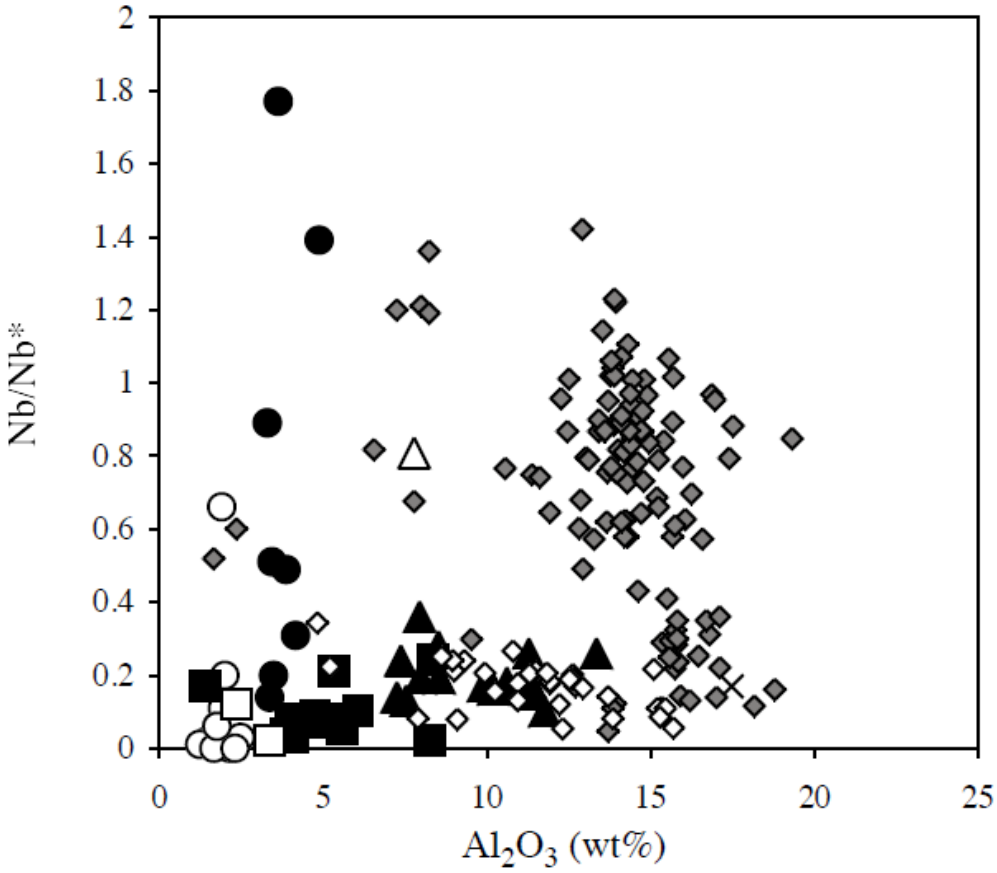

Figure 6

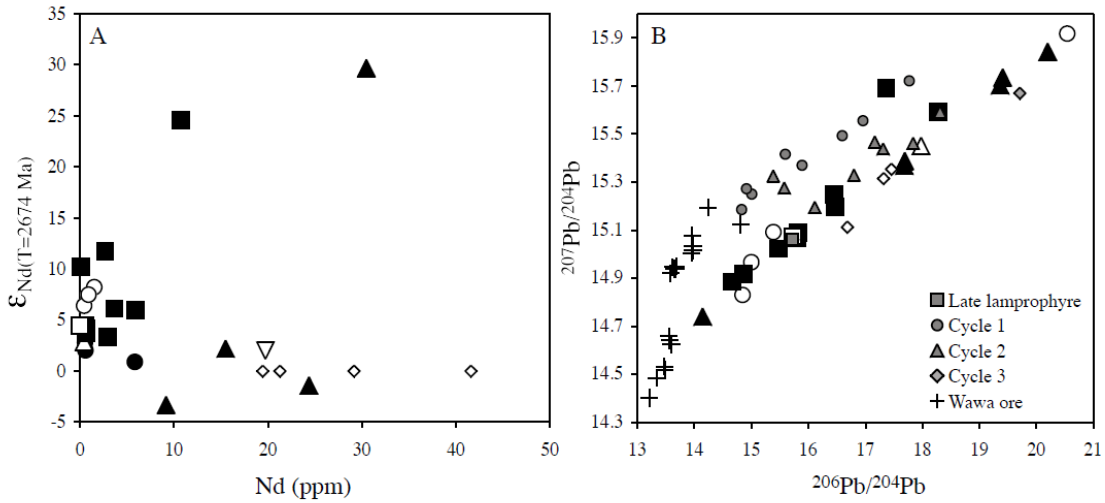

Figure 7

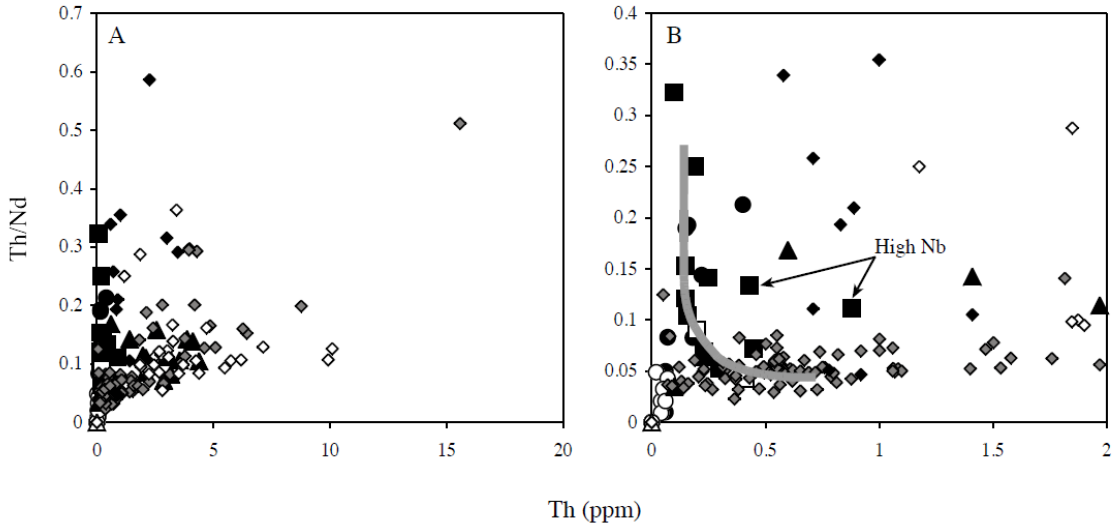

Figure 8

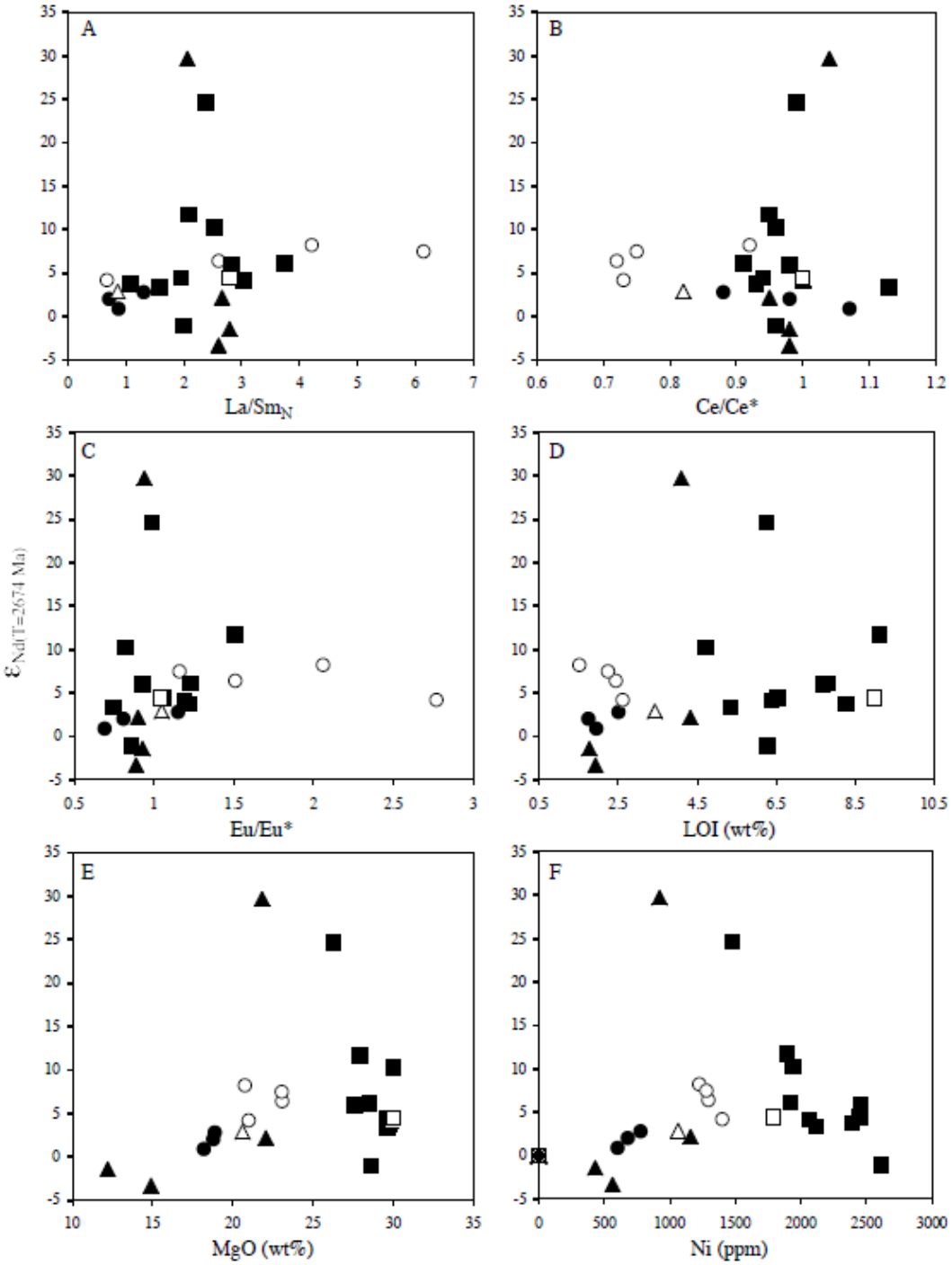

Figure 9

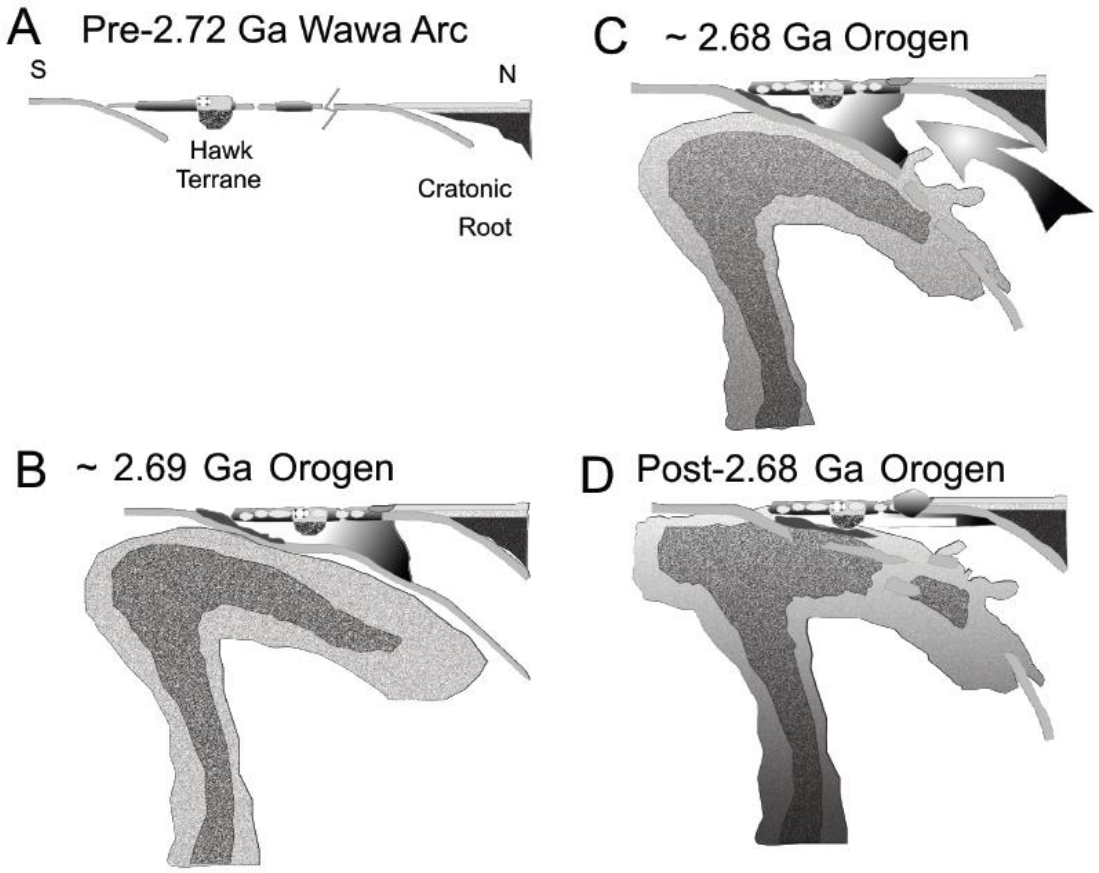

Figure 10

Table 1. Major and trace element abundances for xenoliths in Wawa subprovince lamprophyres

	Group IB (Group 1A in Wyman et al., 2006)								Group II														
Sample #	WX-16	MO10-5	MO10-7	WX30A	GQ10-2	WX-17	WX-19	WX-21	WX-18	WX-22	MO10-1	MO10-2	WX30B	GQ10-3	WX-20	WX31	MO10-3	MO10-6b	MO10-4	WX-15	WX-23	WX-4	WX-5
wt.%																							
SiO_2	53.17	54.49	53.56	54.42	53.8	53.59	53.33	53.2	45.69	48.07	46.94	46.69	48.95	49.13	49.59	48.57	49.1	49.13	45.35	50.26	50.08	49.88	52.9
TiO_2	0.2	0.11	0.16	0.15	0.13	0.17	0.39	0.19	0.23	0.33	1.1	0.98	1.1	1.1	0.97	1.04	0.89	0.35	0.68	0.59	0.94	0.65	0.58
Al_2O_3	4.88	3.44	4.15	3.28	3.35	3.63	3.49	3.87	13.34	7.94	8.51	9.88	11.27	10.19	11.29	10.6	7.24	7.53	11.76	8.54	11.38	7.36	7.97
Fe_2O_3	9.46	7.22	7.97	8.14	9.26	11.01	10.49	11.52	13.27	13.26	11.53	12.73	11.75	11.17	11.01	11.71	12.37	9.7	14.07	12.04	11.34	10.16	9.1
MnO	0.2	0.18	0.18	0.17	0.18	0.25	0.24	0.24	0.18	0.23	0.22	0.19	0.16	0.15	0.15	0.17	0.18	0.17	0.2	0.19	0.15	0.18	0.14
MgO	19.45	22.54	22.28	21.05	20.37	18.77	18.19	18.87	12.32	19.75	21.03	17.81	11.51	15.34	11.79	12.58	17	22.88	19.26	14.91	12.2	21.84	22.06
CaO	9.89	11.2	10.64	11.31	11.67	10.9	12.47	11.36	11.02	9.15	9.94	7.47	9.33	6.33	8.83	9.75	8.93	8.16	7.11	9.09	7.71	9.19	5.59
K_2O	2.7	0.72	0.92	1.38	1.11	1.62	1.24	0.65	3.31	1.09	0.2	3.25	2.58	4.68	3.54	2.76	3.57	1.88	0.8	2.93	3.47	0.15	0.6
Na_2O	0.04	0.07	0.1	0.06	0.1	0.06	0.15	0.08	0.61	0.07	0.09	0.6	2.86	1.42	2.28	2.36	0.44	0.06	0.49	1.19	2.27	0.33	0.87
P_2O_5	0.01	0.02	0.04	0.03	0.02	N.D.	0.01	0.01	0.03	0.09	0.42	0.41	0.48	0.49	0.54	0.46	0.28	0.15	0.28	0.26	0.47	0.26	0.2
LOI	1.72	3.14	3.38	2.36	2.77	1.75	1.95	2.51	2.25	4.11	5.15	3.26	2.89	1.8	2.64	3.68	1.86	4.63	7.08	1.93	1.78	4.1	4.33
Mg#	82	87	86	85	83	79	79	78	67	77	80	75	68	75	70	70	75	84	75	73	70	83	84
ppm																							
Cr	2508	1141	1860	1892	2475	1351	1714	814	777	1801	809	1130	567	744	644	738	1080	1377	1272	1242	651	1265	1372
Co	69	62	67	71	58	93	84	76	65	85	74	71	56	63	59	60	67	69	73	91	59	80	79
Ni	762	1469	1440	1671	1596	679	600	776	446	749	627	616	393	586	411	455	790	1178	791	565	432	921	1157
Rb	112	26	34	50	37	67	50	34	135	43	7	121	85	168	136	99	136	84	20	127	139	3	19
Sr	15	51	54	60	45	19	33	27	936	37	155	177	890	95	386	945	153	51	183	312	327	118	84
Cs	5.82	1.13	1.55	3.26	1.99	3.79	2.36	1.75	6.15	2	0.33	3.63	4.7	8.06	5.97	5.13	4.12	3.68	0.78	5.26	5.89	0.24	0.91
Ba	611	45	69	425	222	400	382	180	801	225	46	809	1114	1195	712	1340	949	185	429	755	709	21	98
Sc	30.1	4.5	5.6	6.9	8.0	32.0	0.0	27.5	44.8	31.9	30.2	28.3	30.8	29.2	30.6	32.5	26.3	13.9	32.9	30.0	31.4	23.1	18.5
V	143	68	107	82	96	138	228	151	278	155	147	218	226	199	230	222	188	140	185	204	232	166	135
Ta	0.07	0.58	0.04	0.07	0.1	0.08	0.04	0.03	0.04	0.07	0.46	0.42	0.3	0.34	0.32	0.29	0.55	0.62	0.35	0.2	0.32	1.33	0.29
Nb	0.81	0.49	0.29	1.75	0.13	0.64	0.4	0.35	0.74	0.82	5.88	3.38	7.7	4.79	5.07	6.36	3.56	1.38	4.99	3.42	4.78	3.82	3.45
Zr	0	—	6.21	7.17	—	0	24.48	0	13.3	22.94	126.52	84.78	89.6	120.18	127.35	97.63	89.66	56.61	131.33	69.34	97.74	75.09	70.04
Hf	0.15	—	0.16	0.19	—	0.21	0.72	0.17	0.31	0.69	3.27	2.21	2.51	3.15	3.28	2.58	2.2	1.38	3.13	1.73	2.51	1.97	1.83
Th	0.15	0.4	0.22	0.18	0.16	0.06	0.06	0.07	0.1	0.6	3.07	2.09	2.87	3.55	4.11	3.16	2.94	1.41	4.39	2.57	3.88	2.11	1.97
U	0.07	0.06	0.05	0.12	0.04	0.16	0.05	0.14	0.08	0.12	0.85	0.5	0.67	0.89	1.31	0.95	0.49	0.31	0.91	0.68	1.09	0.49	0.37
Y	1.69	2.64	2.33	2.23	1	3.66	10.73	3.24	21.98	6.87	20.69	14.42	19.27	19.09	23.31	18.76	12.31	6.15	16.75	14.54	20.2	16.73	11.53
La	0.49	1.23	1.04	1.54	0.65	0.41	2.31	0.54	1.95	2.1	19.22	17.24	27.68	25.41	23.49	30.06	20.75	9.24	40.19	14.2	24.87	13.95	14.31
Ce	1.1	4.27	3.16	3.23	1.23	1.22	7.24	1.12	3.53	5.12	47.32	40.36	68.5	57.04	52.37	67.83	46.53	21.88	90.29	30.26	51.81	33.01	30.37
Pr	0.16	0.4	0.36	0.48	0.19	0.22	1.17	0.18	0.51	0.74	6.26	5.59	9.43	7.73	6.84	9.11	6.2	2.45	10.86	3.9	6.44	4.28	4.14
Nd	0.79	1.88	1.53	2.18	0.83	1.2	6.11	0.84	2.85	3.56	26.72	24.38	39.82	33.37	29.56	38.24	26.17	9.89	41.88	16.24	27.21	19.09	17.23
Sm	0.21	0.51	0.41	0.54	0.22	0.37	1.72	0.27	1.25	1.12	6	5.15	7.91	7.13	6.36	7.51	5.06	1.97	7.03	3.53	5.76	4.37	3.48
Eu	0.07	0.19	0.16	0.12	0.06	0.11	0.41	0.12	0.82	0.32	1.72	1.32	2.21	1.95	1.83	2.02	1.21	0.37	2.24	1	1.68	1.31	0.97
Gd	0.22	0.53	0.42	0.51	0.23	0.47	1.86	0.4	2.19	1.27	5.1	4.02	5.93	5.73	5.5	5.64	3.79	1.57	4.75	3.16	5.03	4.04	2.94
Tb	0.04	0.08	0.06	0.07	0.03	0.08	0.31	0.07	0.45	0.2	0.69	0.53	0.75	0.73	0.76	0.71	0.48	0.21	0.62	0.44	0.69	0.55	0.39
Dy	0.25	0.43	0.37	0.41	0.16	0.63	1.99	0.54	3.53	1.24	4	2.91	4.01	3.94	4.55	3.86	2.51	1.17	3.36	2.67	4.02	3.22	2.28
Ho	0.06	0.09	0.08	0.08	0.03	0.14	0.41	0.12	0.81	0.25	0.75	0.53	0.7	0.72	0.87	0.69	0.45	0.23	0.61	0.53	0.76	0.61	0.42
Er	0.19	0.26	0.24	0.22	0.1	0.43	1.19	0.37	2.58	0.75	2.05	1.44	1.9	1.94	2.51	1.9	1.2	0.64	1.69	1.52	2.06	1.65	1.18
Tm	0.03	0.04	0.04	0.03	0.01	0.07	0.17	0.06	0.39	0.1	0.29	0.2	0.25	0.26	0.36	0.26	0.17	0.09	0.23	0.22	0.29	0.23	0.16
Yb	0.22	0.26	0.23	0.23	0.11	0.47	1.05	0.4	2.61	0.67	1.8	1.24	1.58	1.66	2.28	1.58	1.03	0.62	1.49	1.4	1.87	1.44	1.04
Lu	0.03	0.04	0.04	0.04	0.02	0.07	0.14	0.06	0.4	0.1	0.26	0.19	0.23	0.24	0.33	0.23	0.15	0.1	0.22	0.21	0.26	0.21	0.15
(La/Yb)cn	1.57	3.44	3.22	4.82	4.3	0.62	1.58	0.98	0.54	2.25	7.67	9.94	12.6	11	7.39	13.63	14.4	10.69	19.34	7.27	9.52	6.96	9.83
(La/Sm)cn	1.49	1.57	1.62	1.85	1.88	0.71	0.87	1.31	1.01	1.21	2.07	2.16	2.26	2.3	2.39	2.59	2.65	3.03	3.69	2.6	2.79	2.06	2.66
(Gd/Yb)cn	0.83	1.72	1.51	1.83	1.72	0.82	1.47	0.83	0.7	1.58	2.35	2.67	3.11	2.86	2	2.95	3.04	2.09	2.64	1.87	2.22	2.32	2.33
(La/Y)cn	1.92	3.08	2.94	4.56	4.3	0.74	1.42	1.11	0.59	2.02	6.15	7.92	9.52	8.82	6.67	10.61	11.16	9.94	15.9	6.47	8.16	5.53	8.22
(Tb/Yb)cn	0.75	1.34	1.14	1.39	1.17	0.81	1.35	0.78	0.79	1.37	1.75	1.93	2.15	1.99	1.52	2.05	2.1	1.52	1.88	1.44	1.68	1.72	1.72
(Tb/Y)cn	0.91	1.2	1.04	1.31	1.17	0.97	1.22	0.89	0.87	1.23	1.4	1.53	1.62	1.6	1.37	1.59	1.63	1.41	1.54	1.28	1.44	1.37	1.43
(Eu/Eu*)cn	0.95	1.12	1.17	0.68	0.77	0.81	0.69	1.15	1.5	0.82	0.92	0.86	0.94	0.9	0.92	0.91	0.81	0.63	1.12	0.89	0.93	0.94	0.9
Ce/Ce*	0.95	1.49	1.27	0.92	0.86	0.98	1.07	0.88	0.85	1	1.05	1	1.04	0.99	1	1	1	1.1	1.04	0.98	0.98	1.04	0.95
Nb/Nb*	1.39	0.51	0.31	0.89	0.14	1.77	0.2	0.49	0.26	0.36	0.28	0.17	0.26	0.16	0.18	0.18	0.14	0.13	0.1	0.19	0.15	0.24	0.19

	Group III												Group IV
Sample #	WX-9	WX-13	WX-8	WX-11	WX-12	WX-14	WX-3	WX-1	WX-10	WX-7	WX-2	WX-6	GQ10-4
wt.%													
SiO_2	57.5	56.67	55.41	58.81	58.5	51.71	57.58	56.01	63	52.27	52.83	54.9	36.73
TiO_2	0.1	0.1	0.08	0.06	0.04	0.13	0.06	0.27	0.02	0.11	0.11	0.08	0.23
Al_2O_3	4.75	5.5	4.68	4.04	3.88	8.25	4.08	5.34	1.4	5.59	8.37	6.08	17.46
Fe_2O_3	7.21	8.06	7.47	6.97	6.7	9.38	7.22	7.96	5.48	7.83	9.43	8.28	18.12
MnO	0.06	0.06	0.12	0.05	0.06	0.13	0.11	0.12	0.03	0.18	0.08	0.08	0.2
MgO	29.6	28.65	29.75	29.62	29.88	27.62	28.53	26.26	30.02	27.9	29.12	29.54	22.04
CaO	0.58	0.43	2.32	0.3	0.83	2.43	2.4	3.51	0.03	5.54	0.04	1.04	4.17
K_2O	0.2	0.54	0.17	0.15	0.11	0.35	0.01	0.25	0.01	0.58	0.01	0.01	1.02
Na_2O	0	0	0	0	0	0	0	0.2	0	0	0	0	0
P_2O_5	0	0	0	0	0	0	0.01	0.09	0	0	0.01	0	0.02
LOI	6.53	6.29	8.29	5.35	6.39	7.7	7.79	6.27	4.71	9.13	6.82	7.27	11.83
Mg#	90	89	90	90	91	87	90	88	92	89	87	89	73
ppm													
Cr	2433	2818	3704	2358	2253	3379	1777	1740	614	2736	3152	3604	—
Co	101	103	101	92	92	105	92	82	88	83	108	101	112
Ni	2451	2616	2391	2115	2063	2457	1920	1475	1938	1897	2219	2423	1634
Rb	6	18	6	5	3	12	0	7	0	18	1	0	36
Sr	36	22	209	3	65	74	100	93	1	297	3	48	198
Cs	0.42	1.13	0.44	0.32	0.26	0.93	0.07	0.38	0.05	1	0.11	0.11	6.84
Ba	30	85	30	23	16	68	13	46	1	91	8	3	172
Sc	5.4	1.7	2.4	5.9	2.5	8.9	1.8	8.2	0.0	7.9	1.7	3.0	51.2
V	53	57	54	40	39	97	48	77	15	71	82	69	310
Ta	0.04	0.19	0.08	0.07	0.04	0.15	0.21	1.04	0.05	0.12	0.96	0.13	0.04
Nb	0.06	0.2	0.06	0.06	0.07	0.1	0.26	1.6	0.06	0.15	1.02	0.11	0.33
Zr	0	0	0	0	0	0	6.51	26.67	0	0	11.81	0	15.91
Hf	0	0	0	0	0	0	0.15	0.74	0	0	0.27	0	0.39
Th	0.19	0.23	0.15	0.25	0.16	0.45	0.3	0.88	0.1	0.23	0.43	0.15	0.24
U	0.01	0.03	0	0.01	0.03	0.05	0.85	0.16	0.02	0.03	0.1	0.02	0.08
Y	0.68	1.48	2.09	0.67	0.78	2.61	1.33	5.58	0.15	2.55	0.59	1.15	1.48
La	0.57	2.12	0.72	0.9	1.24	4.91	5.44	6.39	0.27	2.38	2.95	0.86	1.5
Ce	1.19	4.96	1.65	2.78	2.75	10.77	10.33	14.05	0.58	5.07	5.46	1.83	3.14
Pr	0.16	0.76	0.26	0.41	0.35	1.44	1.35	1.87	0.08	0.71	0.8	0.23	0.4
Nd	0.76	3.62	1.24	1.77	1.53	6.3	5.69	7.93	0.31	3.34	3.22	0.98	1.68
Sm	0.19	0.69	0.43	0.37	0.26	1.12	0.94	1.73	0.07	0.74	0.53	0.23	0.31
Eu	0.06	0.17	0.18	0.08	0.09	0.3	0.31	0.53	0.02	0.34	0.11	0.1	0.1
Gd	0.16	0.45	0.46	0.24	0.16	0.76	0.51	1.5	0.05	0.59	0.29	0.2	0.27
Tb	0.02	0.05	0.06	0.03	0.02	0.09	0.05	0.2	0.01	0.07	0.03	0.03	0.03
Dy	0.12	0.27	0.34	0.14	0.12	0.51	0.24	1.12	0.02	0.44	0.13	0.19	0.21
Ho	0.02	0.05	0.07	0.03	0.03	0.1	0.05	0.21	0	0.08	0.02	0.04	0.05
Er	0.07	0.15	0.2	0.07	0.08	0.25	0.14	0.57	0.01	0.24	0.05	0.12	0.16
Tm	0.01	0.02	0.03	0.01	0.01	0.03	0.02	0.08	0	0.04	0.01	0.02	0.03
Yb	0.07	0.15	0.2	0.07	0.1	0.22	0.16	0.5	0.02	0.26	0.06	0.13	0.22
Lu	0.01	0.02	0.03	0.01	0.02	0.03	0.02	0.07	0	0.05	0.01	0.02	0.05
(La/Yb)cn	5.76	10.05	2.59	8.71	9.14	16.32	24.65	9.1	9.81	6.68	37.92	4.66	4.9
(La/Sm)cn	1.96	1.99	1.08	1.59	3.03	2.83	3.74	2.39	2.54	2.09	3.57	2.38	3.09
(Gd/Yb)cn	1.84	2.46	1.89	2.69	1.38	2.9	2.67	2.46	2.18	1.92	4.34	1.23	1.02
(La/Y)cn	5.49	9.48	2.28	8.94	10.53	12.45	27.03	7.59	12.3	6.17	33.12	4.95	6.73
(Tb/Yb)cn	1.31	1.54	1.37	1.75	1.1	1.99	1.37	1.8	1.2	1.31	2.53	1.07	0.68
(Tb/Y)cn	1.25	1.45	1.2	1.8	1.27	1.52	1.5	1.5	1.5	1.21	2.21	1.14	0.94
(Eu/Eu*)cn	1.06	0.86	1.22	0.75	1.19	0.93	1.23	0.99	0.82	1.51	0.77	1.43	1.04
Ce/Ce*	0.94	0.96	0.93	1.13	1	0.98	0.91	0.99	0.96	0.95	0.86	0.99	0.97
Nb/Nb*	0.09	0.08	0.07	0.08	0.04	0.02	0.03	0.21	0.17	0.05	0.24	0.1	0.17

Table 2. Sm–Nd and Pb isotopic results for Wawa xenoliths

Sample #	Sm (ppm)	Nd (ppm)	$^{147}Sm/^{144}Nd$	$^{143}Nd/^{144}Nd$	SE %	eNd (t=today)	eNd (t=2674 Ma)
WX-17	0.187	0.564	0.200412	0.512805	0.000012	3.3	2.0
WX-19	1.607	5.83	0.166697	0.512156	0.000004	-9.4	0.9
WX-21	0.164	0.534	0.186252	0.512589	0.000023	-1.0	2.8
WX-15	1.967	9.156	0.129888	0.511292	0.000014	-26.3	-3.3
WX-23	5.09	24.378	0.126244	0.511325	0.000013	-25.6	-1.4
WX-4	3.488	30.474	0.069203	0.511901	0.000007	-14.4	29.7
WX-5	3.171	15.472	0.123925	0.511465	0.000007	-22.9	2.2
WX-9	0.127	0.545	0.140896	0.511877	0.000008	-14.9	4.4
WX-8	0.206	0.622	0.200265	0.512888	0.000024	4.9	3.7
WX-11	0.612	2.98	0.124251	0.511528	0.000013	-21.7	3.3
WX-12	0.12	0.669	0.108156	0.511291	0.000009	-26.3	4.1
WX-14	0.996	5.905	0.102019	0.511268	0.000014	-26.7	5.9
WX-3	0.583	3.658	0.09642	0.51118	0.000008	-28.5	6.1

Sample #	$^{206}Pb/^{204}Pb$	SE %	$^{207}Pb/^{204}Pb$	SE %	$^{208}Pb/^{204}Pb$	SE %
WX-18	14.14954	0.00248	14.73959	0.00159	33.86114	0.00248
WX-22	19.41407	0.003203	15.73671	0.002013	38.93634	0.003203
WX-15	19.3632	0.004238	15.70269	0.002672	39.45672	0.004238
WX-23	20.2044	0.003726	15.84374	0.002344	39.45998	0.003726
WX-4	17.6842	0.002347	15.36908	0.001541	36.36745	0.002347
WX-5	17.69551	0.002956	15.38778	0.001903	37.17981	0.002956
WX-8	14.65513	0.002523	14.88475	0.001677	34.63218	0.002523
WX-11	16.44347	0.003886	15.24648	0.002489	36.94667	0.003886
WX-12	15.48622	0.003748	15.02282	0.002418	35.56151	0.003748
WX-3	15.82234	0.002885	15.0874	0.001915	35.23095	0.002885
WX-1	16.47211	0.002633	15.19696	0.001683	36.13098	0.002633
WX-10	18.28584	0.004255	15.59363	0.003983	38.32444	0.006147
WX-7	14.86212	0.003305	14.917	0.002152	34.86541	0.003305
WX-2	17.3674	0.006206	15.69198	0.003945	39.16218	0.006206

Highlights

So-called kimberlite indicator minerals derived from lamprophyres

Xenoliths in 2.67 Ga lamprophyres represent shallow mantle arc-related lithologies

No evidence of deep keel identified in xenoliths from younger kimberlites or from geophysics

Implies late amalgamation of cratonic root and greenstone crust

Orogenic Au mineralization predated local keel